



All Theses and Dissertations

2011-06-13

Investigating a Model Reversed-Phase Liquid Chromatography Stationary Phase with Vibrationally Resonant Sum Frequency Generation Spectroscopy

Arthur D. Quast

Brigham Young University - Provo

Follow this and additional works at: <https://scholarsarchive.byu.edu/etd>

 Part of the [Biochemistry Commons](#), and the [Chemistry Commons](#)

BYU ScholarsArchive Citation

Quast, Arthur D., "Investigating a Model Reversed-Phase Liquid Chromatography Stationary Phase with Vibrationally Resonant Sum Frequency Generation Spectroscopy" (2011). *All Theses and Dissertations*. 2764.
<https://scholarsarchive.byu.edu/etd/2764>

This Thesis is brought to you for free and open access by BYU ScholarsArchive. It has been accepted for inclusion in All Theses and Dissertations by an authorized administrator of BYU ScholarsArchive. For more information, please contact scholarsarchive@byu.edu, ellen_amatangelo@byu.edu.

Investigating a Model Reversed-Phase Liquid Chromatography Stationary Phase with
Vibrationally Resonant Sum Frequency Generation Spectroscopy

Arthur D. Quast

A thesis submitted to the faculty of
Brigham Young University
in partial fulfillment of the requirements for the degree of
Master of Science

James E. Patterson, Chair
Steven R. Goates
Milton L. Lee

Department of Chemistry and Biochemistry
Brigham Young University

August 2011

Copyright © 2011 Arthur D. Quast

All Rights Reserved

ABSTRACT

Investigating a Model Reversed-Phase Liquid Chromatography Stationary Phase with Vibrationally Resonant Sum Frequency Generation Spectroscopy

Arthur D. Quast

Department of Chemistry and Biochemistry, BYU

Master of Science

Reversed-phase liquid chromatography (RPLC) is a widely used technique for analytical separations but routinely requires empirical optimization. Gaining a better understanding of the molecular reasons for retention may mean more efficient separations with fewer trial and error runs to obtain optimized separations. Vibrationally resonant sum frequency generation (VR-SFG) is a surface specific technique that has allowed for *in situ* examination of model RPLC stationary phases under various solvent and pressure conditions. In order to improve on past work with model RPLC stationary phases two challenges had to be overcome. First, improved vibrational mode assignments of the C18 stationary phase were needed for proper understanding of this model system. Second, the synthesis of back-surface reference mirrors used in these VR-SFG experiments allowed us to better correct the relative intensities of the various spectral peaks present in typical spectra. After examination of model RPLC systems under various conditions, we have found that these model substrates have a significant amount of interference from nonresonant signal. This interference of resonant and nonresonant signals on fused silica surfaces has not been previously examined and further studies of the model RPLC stationary phase must properly deal with the non-negligible nonresonant interference that is present. We have seen changes in the VR-SFG spectra of these model systems under a variety of conditions including elevated pressure, however the changes are mostly due to nonresonant interference. These spectral changes, although apparently not solely from structural changes, need to be investigated further to better understand the molecular basis of retention in model RPLC systems.

Keywords: reversed-phase liquid chromatography, sum frequency generation, vibrationally resonant sum frequency generation, back surface gold mirrors, variable time delay

ACKNOWLEDGEMENTS

I could never have had the success I have enjoyed in this program without the loving support of my wife, Stacie, who has been a tireless cheerleader on my behalf. Stacie, Annie, my family, and close friends have given me so many reasons why trying my hardest is so worth it. I would not be writing this thesis without their support and love for which I will always be grateful. I remember visiting with Dr. Patterson after taking his physical chemistry class to discuss research in his lab almost 4 years ago. I would never have imagined then that I would be completing a masters degree or that I could have learned so much. Dr. Patterson has been an exceptional advisor and mentor these past two years. I feel very lucky to have been a part of his group. I have learned so much working with and being taught by him. I am also grateful to the many colleagues and friends that I have made while completing this program. I am very glad to have had the pleasure to associate with so many kind and friendly individuals. My academic growth is in large part due to the difficult course work that I have been exposed to and the many wonderful teachers in this department. Thank you.

Table of Contents

Chapter 1: Understanding the Molecular Basis of Retention in RPLC Systems	
1.1 RPLC: The Workhorse of Separations.....	1
1.2 Trial and Error: The Chromatographer's Daily Struggle	2
1.3 Attempts at a Molecular Based Understanding: Theory and Models	3
1.4 Spectroscopic Investigations with Raman and IR: What We Have Learned	4
1.5 VR-SFG: An Inherently Interface-Specific Technique	10
1.6 VR-SFG: A Coherent Probe	10
1.7 The Second Order Non-linear Susceptibility, $\chi^{(2)}$	11
1.8 VR-SFG: Energy Diagram	16
1.9 Orientation Analysis of VR-SFG Spectra	17
1.10 Interference of χ_R and χ_{NR}	21
1.11 VR-SFG: Past RPLC Studies	24
1.12 VR-SFG: Present work	27
1.13 References	31
Chapter 2: Improved Assignment of Vibrational Modes for Surface-Bound Alkylsilanes	
2.1 Background	33
2.2 Experimental and Computational Methods	34

2.2.1 Synthesis of Deutero-Substituted Molecules.....	34
2.2.2 Sample Preparation for Spectroscopic Characterization	37
2.2.2a FTIR Analysis	37
2.2.2b VR-SFG Analysis	37
2.2.3 VR-SFG System	38
2.2.4 Computational Methods	39
2.3 Results and Discussion	39
2.3.1 FTIR Spectra	39
2.3.1a CH Stretching Region	39
2.3.1b CD Stretching Region.....	40
2.3.1c Fingerprint Region	41
2.3.2 DFT Calculations	41
2.3.3 VR-SFG Spectra: <i>ssp</i> vs. <i>sps</i>	46
2.3.4 Variable Time Delay VR-SFG Spectra: <i>ssp</i>	46
2.3.5 VR-SFG of ODMS and DMS	46
2.4 Additional Discussion and Conclusions	50
2.5 References	55
 Chapter 3: Back-Surface Gold Mirrors for Vibrationally Resonant Sum-Frequency (VR-SFG) Spectroscopy Using 3-Mercaptopropyltrimethoxysilane as an Adhesion Promoter	
3.1 Introduction	56

3.2 Experimental Methods	60
3.3 Results and Discussion	63
3.3.1 Importance of Reference Spectra	63
3.3.2 Unsuccessful Attempts to Make Stable Back-Surface Gold Mirrors	65
3.3.3 Successful Attempts to Make Stable Back-Surface Gold Mirrors	68
3.3.4 Use as a Spectroscopic Reference	70
3.4 Use as a Spectroscopic Reference	71
3.5 Conclusions	77
Chapter 4: Understanding Stationary Phase Structure at the RPLC Interface with VR-SFG	
4.1 Introduction: VR-SFG and Nonresonant Interference	79
4.2 Experimental	81
4.3 Results and Discussion	81
4.3.1 Delay Stage Reproducibility	81
4.3.2 Changes in Polymeric Structure in Air at Various Visible Delays	82
4.3.3 Changes in Polymeric Structure under Solvent at Ambient Pressure	87
4.3.4 Polymeric Stationary Phases at 900 psi in H ₂ O	88
4.3.5 Polymeric Stationary Phases at Pressures Above 900 psi	94
4.4 Conclusions	95
4.4 References	98

Chapter 5: Conclusions and Afterthoughts

5.1 Structure of the RPLC Stationary Phase	99
5.2 Gold Mirrors	100
5.3 RPLC	101
5.4 Pressure Work	101
5.5 References	102

Chapter 1

Understanding the Molecular Basis of Retention in RPLC Systems

1.1 RPLC: The Workhorse of Separations

Analytical chromatography has been dominated for many years by reversed-phase liquid chromatography (RPLC). Between 80 and 90% of all analytical separations involve the use of RPLC.¹ It is hard to overstate the importance that RPLC has in modern separation science and its wide use in chemical separations is easily noted in any analytical laboratory.

In general, RPLC includes any separation method that has a nonpolar stationary phase and a polar mobile phase. The stationary phase is commonly comprised of fused silica particles that have been functionalized with nonpolar hydrocarbon chains. These hydrocarbon chains are often identified by how many carbon atoms they contain in each fully saturated chain. Stationary phases coated with chains of one, five, or eighteen carbons would typically be designated as C1, C5, or C18 phases, respectively. The coated fused silica particles are then packed into a stainless steel column. Separations are then performed by flowing a mobile phase, containing the molecules to be separated, through the column.

The most common mobile phase is typically comprised of water, acetonitrile, methanol, or a mixture of these solvents, although, other solvents are used in RPLC separations. Separation of analyte (or solute) molecules occurs as different molecules exhibit dissimilar affinities for the stationary phase. A molecule's retention on the column is related, among other properties, to its hydrophobicity. Those molecules that leave, or elute, first are considered to be less retained by the column than those that elute later. So a very hydrophobic molecule is likely to elute much later than a molecule that is more hydrophilic in nature.

This simple system involving a nonpolar phase and a polar phase is the separation method of choice for two reasons. These coated particles that make up the stationary phase exhibit excellent mass transfer properties for solute molecules and they are relatively easy to make reproducibly. These stationary phases also exhibit excellent chemical stability at reasonable temperatures and near neutral pH. Although, there are some differences between similarly made stationary phases, for the most part, these phases can be readily reproduced and reused many times. With such a large variety of organic molecules being separated with RPLC, its dominance in the separations field is sure to continue for many years to come.

1.2 Trial and Error: The Chromatographer's Daily Struggle

In spite of its regular use in separating compounds, RPLC has some difficulties that still persist. Some of these issues include the need for empirical optimization and day-to-day changes in retention times. Even with these problems, RPLC is a clear winner when it comes to being able to separate organic compounds. If however, these problems could be better understood and possibly eliminated, RPLC might be even more efficient than it is now.

Chromatographers frequently need to calibrate their columns with standard mixtures and adjust the mobile phase composition to separate mixtures of molecules, even if they already know something about the properties of those molecules. This is far from the ideal situation in which the RPLC system is understood at a molecular level. Such an understanding may pave the way for more accurate RPLC systems where inexperienced users perform day-to-day separations. Instead of needing more expert chromatographers to run RPLC systems, it may be that the solution to these problems lies in understanding how retention occurs.

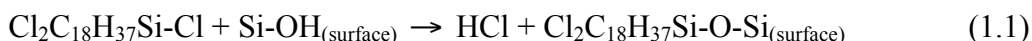
1.3 Attempts at a Molecular Based Understanding: Theory and Models

Because RPLC plays such an important role in analytical separations, there have been many efforts to understand retention of analyte molecules in reversed-phase columns at a molecular level. Since the invention of RPLC in the 1950's,² there has been notable work towards understanding how the interactions between the stationary phase, mobile phase, and analytes influence separations; however, more work is needed.

To properly exploit the potential of RPLC, a sound molecular-based understanding of this system is a goal for many researchers. Dorsey and Dill published theoretical work more than two decades ago in an attempt to explain the retention of analytes on a typical RPLC column. Although much of their research has a different focus from this work's main objective, one central idea that arises from Dorsey and Dill is that of the stationary phase's interphase region where the stationary phase interacts with the mobile phase and solute molecules.³ The idea that the stationary phase's long hydrocarbon chains exhibit an ordered structure with which solute molecules interact is central to understanding retention.

These chains must exhibit some ordering because of 2 constraints placed on them by their attachment to the fused silica particles. The point of attachment means that the orientation at the surface must be limited. They must generally point away from the particle surface because they cannot extend into the solid support they are attached to. Also, the presence of neighboring chains limits each chain's conformation. A typical model of this structure at the solid/liquid interface is given in Figure 1.1, reproduced from Dorsey et al.¹ This model in which the solute molecules are retained on the RPLC column as they adsorb on the surface or interact with spaces between chains is not the complete picture. These hydrocarbon chains are free to bend at various distances throughout the chain length.

Figure 1.2 shows typical C18 stationary phases bonded to fused silica through silanol linkages. This bonding is typical for RPLC stationary phases and occurs as a molecule such as trichlorooctadecylsilane loses a Cl group and bonds with a free silanol on the surface of the fused silica as in reaction 1.1:



The attached silane can undergo two additional reactions to produce a surface bonded C18 group, where all three bonds with the C18 silane are between the chain and the surface or a polymeric phase, which is bonded to other C18 chains many times. It is easily seen that the simplistic view in Figure 1.1 is not the only possibility. The C18 chains in Figure 1.2 can also bend at methylene units, transforming the chains from an all trans configuration to one having any number of gauche defects or chinks in the chain.

Another possible model of the stationary phase structure in which the stationary phase chains are allowed to bend and move is shown in Figure 1.3, from the same reference as Figure 1.1. Here we see the ability of C18 chains to bend and “breathe” within the confines of the chemisorbed bonds to the surface. Another insight that this model provides is the ability of solute molecules to interact with the C18 chains, which change conformation when they interact with passing solute molecules in the mobile phase. This picture of the stationary phase as an interphase is a more modern picture of the structure of the RPLC interface. (Figure 1.3)

1.4 Spectroscopic Investigations with Raman and IR: What We Have Learned

Although these models are a good start to understanding the interplay between stationary phase structure changes and retention of solute molecules, they are still only conceptual models. In an effort to understand the changing structure of the stationary phase and how it is influenced

by the mobile phase, several researchers have used linear spectroscopic techniques, such as Raman and IR spectroscopy, that are able to examine the actual surface bonded C18 chains.

Pemberton et al. used Raman spectroscopy to investigate common C18 stationary phases.^{4,5} By exposing RPLC packing material to typical pressures, solvent compositions, buffer compositions, and temperatures, these workers were able to observe changes in stationary phase structure with different experimental conditions. This work is important because it actually examined the stationary phase after it had been exposed to typical LC conditions, although it was not *in situ*. One of the most interesting parts of this work was the observation that polar solvents seemed to induce a more ordered C18 structure, while nonpolar solvents had the opposite effect of opening up the C18 chains. These changes in C18 chain ordering were determined by examining the energy shifts of methylene stretches in the Raman spectra. Although these changes seem to agree with theory, the apparent shifts and spectral changes are very subtle to the average observer.

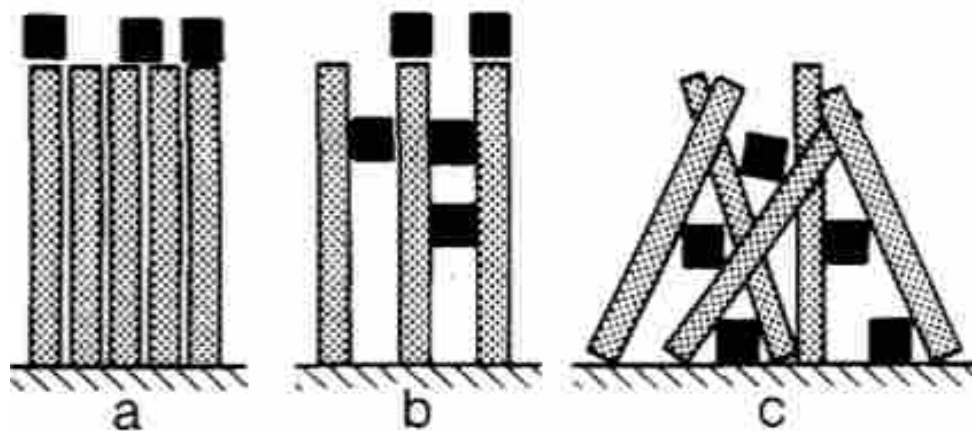


Figure 1.1. A simplistic interpretation of the RPLC stationary phase as a (a) picket; (b) fur; or (c) stack structure. Reproduced with permission from publisher.¹

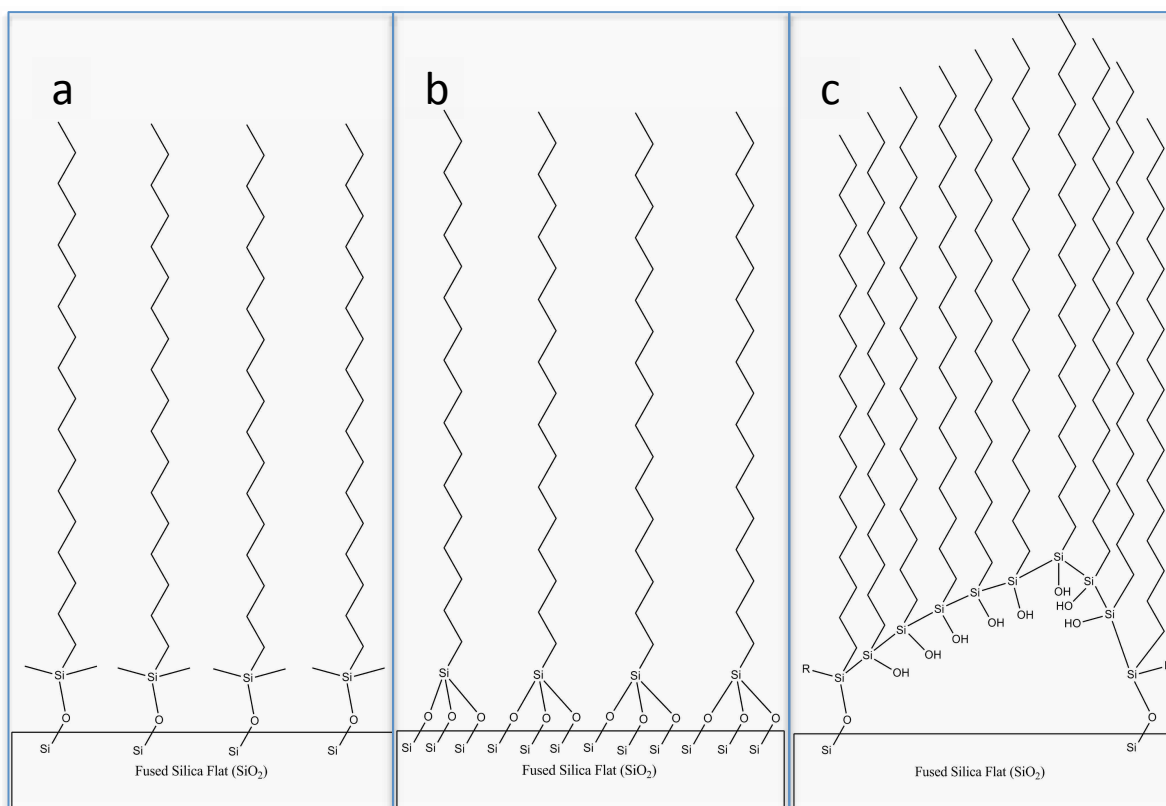


Figure 1.2. The basic stationary phase structure in RPLC is made of long alkyl chains that are bound to the bulk silica surface through silanol linkages (Si-O-Si). (a) Monomeric C18 stationary phase; (b) Surface bound polymeric C18 stationary phase; (c) Polymerized densely packed C18 stationary phase.

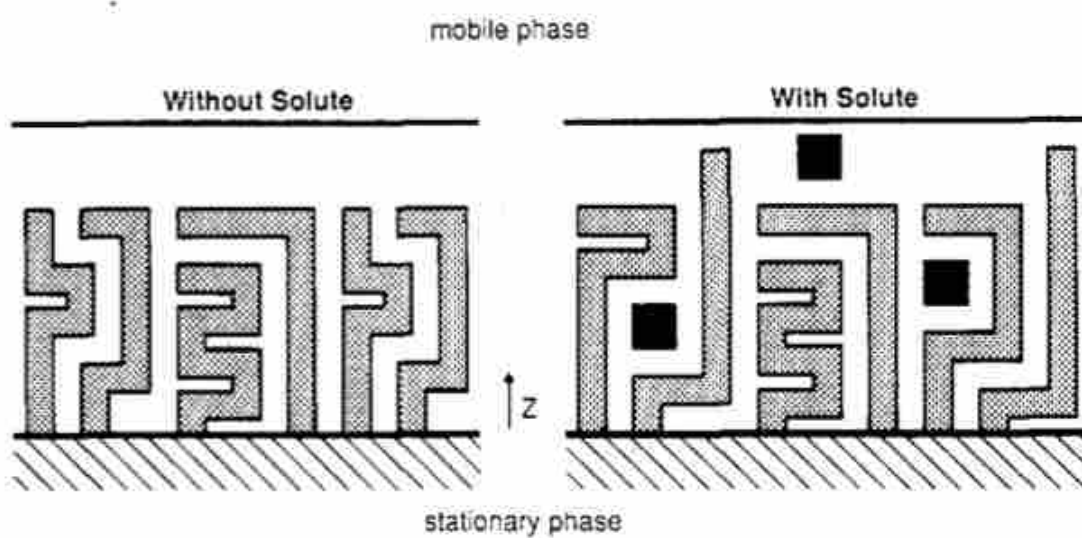


Figure 1.3. The interphase model shows a changing stationary phase with the presence of solute molecules. Reproduced with permission from publisher.¹

Infrared spectroscopy has also been used to investigate the structure of the RPLC interface.⁶ Sander et al. investigated the degree of surface coverage of polymeric C18 stationary phases coated under different conditions and noted that as the surface coverage increased the conformational order also increased. This observation was made using the amplitude of the high-energy methylene antisymmetric stretch and the methylene wag mode. The changes seen in Sander's work also agree with theoretical models and seem to be more apparent than Perberton's Raman work.

Raman and IR spectroscopy are undoubtedly versatile and useful techniques, but they also have the same inherent disadvantage. RPLC separations are surface-specific. The mass transfer that occurs between the stationary and mobile phases is at the stationary phase surface and so Raman and IR spectroscopy are not the most ideal for probing surface phenomena, because they are not particularly sensitive to surface structural changes. Additionally the full RPLC retention story should be told while the stationary phase is being exposed to typical RPLC conditions, *in situ*. We cannot assume that whatever changes occur in the stationary phase while under solvents at elevated pressures will still exist when the solvent and pressure are gone.

The most relevant study of the RPLC stationary phase should use a technique that is both surface specific and can be used *in situ*. Vibrationally resonant sum frequency generation (VR-SFG) is ideal for this work.⁷ VR-SFG meets both of the above criteria while also being a coherent technique, meaning it does not scatter in any direction and the produced light has the same phase. Another advantage that VR-SFG has over Raman and IR spectroscopy is that it is sensitive to molecular orientation.

1.5 VR-SFG: An Inherently Interface Specific Technique

SFG is a nonlinear optical technique that can be used to probe vibrational transitions of molecules ordered at an interface.⁸ SFG arises from the dielectric polarization:

$$P(t) \propto \chi^{(1)}E(t) + \chi^{(2)}E^2(t) + \chi^{(3)}E^3(t) + \dots \quad (1.2)$$

where χ is the material's susceptibility to an electric field. $E(t)$ is the electric field at a given instant in time. The first term in equation 1.2 gives rise to linear optical processes such as infrared and Raman transitions. The second term gives rise to second order nonlinear optical phenomena such as sum and difference frequency generation. The third term gives rise to higher order optical processes, which will not be discussed here. The intensity of SFG produced by a material is dependent on $\chi^{(2)}$ and the two input electric fields E_{ω_1} , and E_{ω_2} .

$$I_{SFG} \propto \left| \chi^{(2)} E_{\omega_1} E_{\omega_2} \right|^2 \quad (1.3)$$

I_{SFG} , E_{ω_1} , and E_{ω_2} are the intensity of the SFG and the electric fields of the ω_1 and ω_2 , respectively.⁹ From equations 1.2 and 1.3, we see that the SFG beam is dependent on the square of the intensities of the two fundamental light pulses that combine to form the SFG pulse.

1.6 VR-SFG: A Coherent Probe

One notable advantage that SFG has over linear techniques is that SFG uses two coherent pulses of light to produce a third coherent pulse, which is easier to collect and detect. For SFG to occur, two frequencies of light, ω_1 and ω_2 , combine at an interface to produce ω_{SFG} at the sum of the two input frequencies:

$$\omega_1 + \omega_2 = \omega_{SFG} \quad (1.4)$$

Because both energy and momentum are conserved with the SFG pulse, the angle at which the pulse leaves the sample can be known if the incident angles of ω_1 and ω_2 are also known (Figure 1.4). If we write the x-momentum of the SFG beam as the sum of the x-momenta of E_1 and E_2 ,

then we have:

$$\omega_1 \cos \theta_1 + \omega_2 \cos \theta_2 = \omega_{SFG} \cos \theta_{SFG} \quad (1.5)$$

where θ_1 , θ_2 , and θ_{SFG} are the angles of incidence and reflection of ω_1 , ω_2 , and ω_{SFG} , respectively. Equation 1.5 is easily rearranged to yield θ_{SFG} :

$$\theta_{SFG} = \frac{\cos^{-1}(\omega_1 \cos \theta_1 + \omega_2 \cos \theta_2)}{\omega_{SFG}} \quad (1.6)$$

1.7 The Second Order Non-linear Susceptibility, $\chi^{(2)}$

In addition to energy and momentum being conserved, SFG can only be produced at an interface as a result of phase matching conditions arising from the 3rd rank tensor, $\chi^{(2)}$. Where $\chi^{(2)}$ is a 27-element tensor that describes the nonlinear susceptibility in a given 3-dimensional space (Figure 1.5).⁸ If the space that is described by $\chi^{(2)}$ is isotropic, meaning there is no preferred direction, then all 27 elements of $\chi^{(2)}$ are identically zero.

In an anisotropic space, like an interface, some of the elements become zero and some do not. Let us consider an arbitrary surface, and on that surface we place the Cartesian coordinates of x, y, and z (Figure 1.6). We define z to be parallel with the surface normal. If we perform a 180° rotation about the z-axis, we can see that the vectors x and y become -x and -y (Figure 1.6a). This means that elements of the $\chi^{(2)}$ tensor which have an odd number of x's or y's must be zero for an azimuthally symmetric interface. If we pick $\chi^{(2)}_{(xyy)}$ then the only way this element can equal $\chi^{(2)}_{(-x)(-y)(-y)}$ is if $\chi^{(2)}_{(xyy)} = \chi^{(2)}_{(-x)(-y)(-y)} = 0$. By similar inspection, we find that $\chi^{(2)}$ reduces from 27 elements to only 13.

If we then perform a 90° rotation about the z-axis (Figure 1.6b) then we see that x = y and x = -y. This operation yields 6 relationships: $\chi^{(2)}_{xyz} = \chi^{(2)}_{yxz}$, $\chi^{(2)}_{xzy} = \chi^{(2)}_{yzx}$, $\chi^{(2)}_{xxz} = \chi^{(2)}_{yyz}$, $\chi^{(2)}_{zxx} = \chi^{(2)}_{zyy}$, and $\chi^{(2)}_{zxy} = \chi^{(2)}_{zyx}$. If a mirror plane including the z-axis is considered, we see that the vectors x and -y transform to y and -x, as well as the vectors -x and

–y transform to x and y (Figure 1.6c). This reasoning leads to $\chi^{(2)}$ being reduced to only 7 non zero terms, only 4 of which are independent.

Now that we understand which elements of $\chi^{(2)}$ can be nonzero, we will discuss how we represent these elements in a laboratory frame of reference. Plane polarized light that includes the z-axis is defined to be p polarized, and plane polarized light that is perpendicular to the z-axis is defined to be s polarized. This analysis is true of any interface and demonstrates the allowed polarizations for SFG that result in the $\chi^{(2)}$ tensor being nonzero.

In summary, the usefulness of SFG and its ability to generate signal from these buried interfaces results from the isotropic symmetry of bulk materials being broken at interfaces. The non-linear susceptibility, a third rank tensor, is equal to zero if the probed environment is isotropic, and is nonzero if the environment is anisotropic. The anisotropic second order non-linear susceptibility, $\chi^{(2)}$, has 7 non-vanishing elements which correspond to the allowed combinations of $\chi^{(2)}$: χ_{zzz} , $\chi_{xzx} = \chi_{yzy}$, $\chi_{zxx} = \chi_{zyy}$, and $\chi_{xxz} = \chi_{yyz}$. These allowed polarizations are by convention listed in descending order of energy and are hereafter referred to as *ppp*, *sps*, *pss*, and *ssp*.

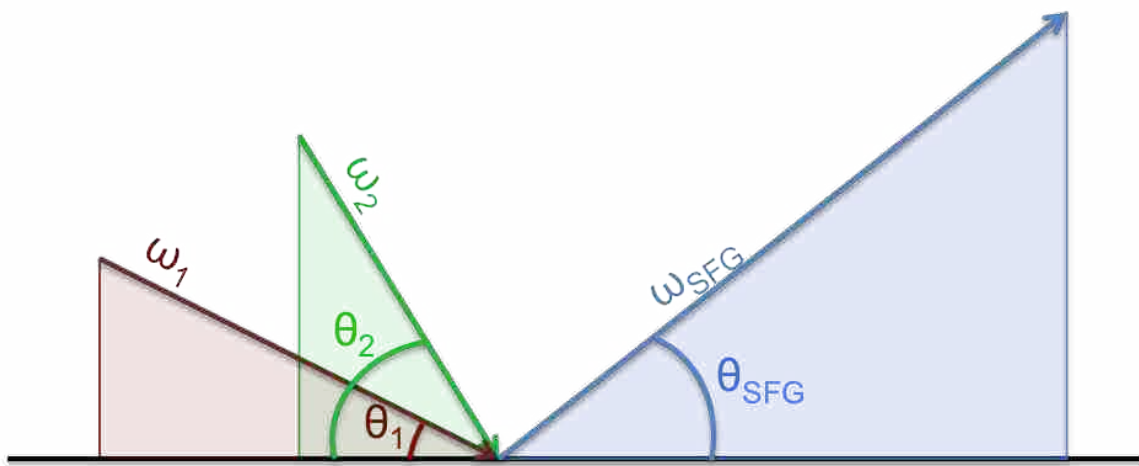


Figure 1.4. Energy and momentum are conserved as ω_1 and ω_2 combine on an interface to produce ω_{SFG} at incident angles of θ_1 and θ_2 as well as θ_{SFG} which is reflected.

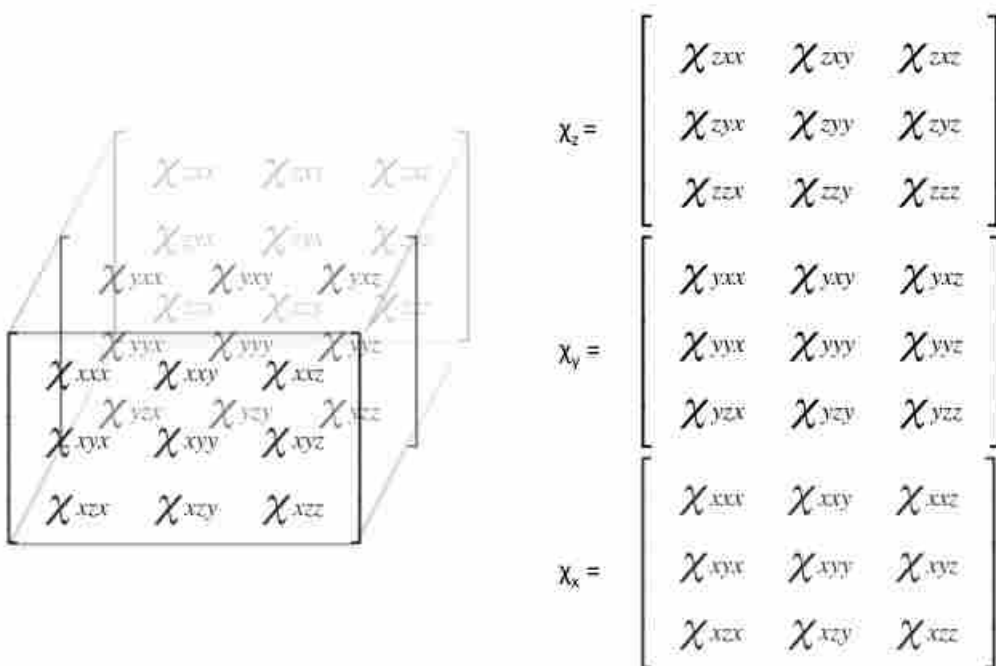


Figure 1.5. The second order nonlinear susceptibility $\chi^{(2)}$ with 27 elements. $\chi^{(2)}$ is a 3rd rank tensor describing the nonlinear susceptibility in 3 dimensions.

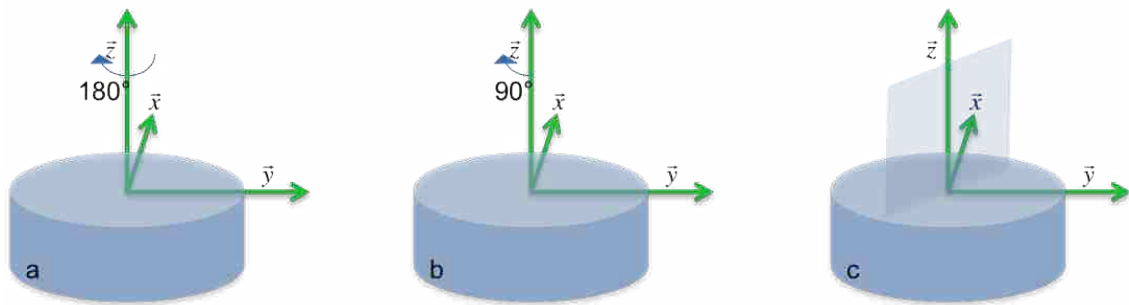


Figure 1.6. An arbitrary interface/surface with a coordinate axis on top. (a) 180° rotation about z axis, (b) 90° rotation about z axis (c) mirror plane including the z axis.

1.8 VR-SFG: Energy Diagram

Understanding that VR-SFG arises from interfaces and that it is a coherent source of light, we can now examine how these two pulses of light, ω_1 and ω_2 , mix at a surface and provide useful molecular information. Let ω_1 and ω_2 be an infrared and visible pulse, ω_{IR} and ω_{vis} . If we imagine a molecule at the interface, where ω_{IR} and ω_{vis} mix spatially and temporally, a resonant vibrational transition can be excited. This occurs when the IR pulse is the same frequency as the molecular vibration. The excited molecule then interacts with the visible electric field. This can be thought of as exciting the molecule from the ground vibrational state, a, to an excited vibrational state, b, with ω_{IR} (Figure 1.7). This excited molecule is then again excited to a virtual state, c, with ω_{vis} , which then decays in an antistokes Raman fashion to produce a coherent SFG pulse at the sum of the two fundamental energies. We can imagine this transition as a vibrational excitation and then an antistokes Raman scattering event. However, it is better to consider this to be a concerted transition instead of happening sequentially.

A resonant enhancement of the VR-SFG pulse is obtained if these transitions caused by the visible and infrared pulses overlap with real states. Equation 1.6 explicitly states this¹⁰

$$\chi_{ijk}^{(2)} \propto \chi_{NR} + N \sum_{a,b,c} \frac{\langle a | \mu_i | c \rangle \langle a | \mu_j | b \rangle \langle b | \mu_k | c \rangle}{(h\omega_{SFG} - E_{ca} - i\Gamma_{ca})(h\omega_{IR} - E_{ab} - i\Gamma_{ab})(h\omega_{vis} - E_{bc} - i\Gamma_{bc})} \quad (1.6)$$

here, N is the number density of surface molecules; h is Plank's constant; E_{ca} , E_{ab} , and E_{bc} are the energies of the transitions in the visible, infrared, and visible, respectively; μ is the dipole operator; and Γ is the line width for each of the transitions. The subscripts on χ are the input (j,k) and output (i) fields having any combination of Cartesian coordinates (x,y,z). χ_{NR} is the nonresonant portion of the 2nd order nonlinear susceptibility. If we use electromagnetic fields that

have energies close to the resonant transitions of surface molecules, then the denominator in the summation term becomes small and $\chi_{ijk}^{(2)}$ becomes resonantly enhanced.

This resonant enhancement is exploited heavily in the field of VR-SFG, although usually only two of the three states are real as in Figure 1.7. Equation 1.7 illustrates the most typical use of VR-SFG.

$$I_{SFG} \propto \left| \chi_{NR}^{(2)} + \chi_R^{(2)} \right|^2 = \left| B_{NR} e^{i\phi} + \sum_q \frac{A_q}{\nu_{IR} - \nu_q - i\Gamma_q} \right|^2 \quad (1.7)$$

B_{NR} is the amplitude of the nonresonant contribution; $e^{i\phi}$ states the interference of the resonant and nonresonant signals with the phase factor ϕ ; and the terms A_q , ν_q , and Γ_q are the amplitude, center frequency, and half-height, half-line-width, respectively, of resonant features having Lorentzian line shapes. When we excite these vibrational transitions through VR-SFG, we obtain an up-converted vibrational spectrum of the molecule at the interface. By subtracting the energy of the visible pulse from the SFG pulse energy, we can easily visualize this visible SFG spectrum as an infrared spectrum.

1.9 Orientation Analysis of VR-SFG Spectra

When the infrared pulse is overlapped with the CH stretching region of surface molecules at the RPLC interface, we can obtain the relative orientation of these C18 chains. This is accomplished by comparing the relative intensities of the various modes observed with VR-SFG. For a RPLC stationary phase, there are four stretching modes that are typically used when determining molecular orientation. These modes are the methyl symmetric, r^+ ; the methyl antisymmetric, r^- ; the methylene symmetric, d^+ ; and the methylene antisymmetric, d^- , stretching modes. The absence of the d^+ and d^- modes indicates that the C18 chain is in an all trans configuration, such as the structure in Figure 1.2. When these modes have large amplitudes in the

VR-SFG spectrum, this indicates that the C18 chain has a number of gauche defects, and we consider this to show disorder in the stationary phase structure.

The methyl modes can be used to determine the terminal methyl tilt angle. Let us imagine an electric field that is parallel to the surface normal. If the symmetric transition dipole moment for the methyl group is parallel to this electric field, then it oscillates well with the electric field. The antisymmetric dipole transition is perpendicular to this electric field and is not excited. We can examine further tilt angles of the C18 chain and how the tilt affects the excitation of the terminal methyl group. Figure 1.8 is reproduced from a study involving self assembled monolayers (SAM's) of octadecanethiol (ODT) on gold.¹¹ By taking the ratio of r^+ and r^- , we can determine the tilt angle of the C18 chain having an all trans configuration.

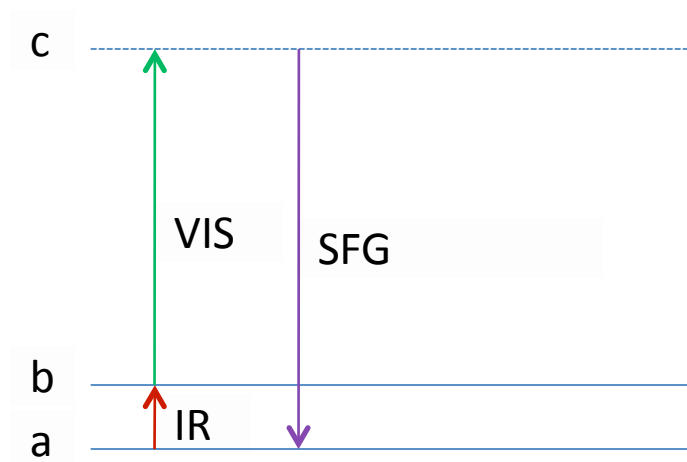


Figure 1.7. The energy level diagram for IR-VIS SFG involving a, b, and c as two real states and a virtual state, respectively. The SFG signal is produced as an infrared and a visible pulse mix at an interface in a concerted non-linear fashion.

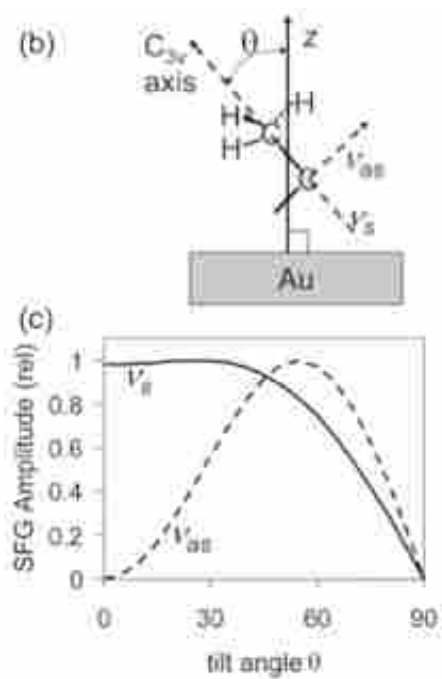


Figure 1.8. The VR-SFG amplitudes of the terminal methyl group stretches change as the C18 chain's tilt angle moves with respect to the surface normal.¹¹

1.10 Interference of χ_{NR} with χ_R

Recently, researchers working with VR-SFG have had to sort out what effect, if any, the nonresonant portion of the SFG signal may have on their claim that VR-SFG can be used for absolute orientation analysis. Lagutchev et al. observed that if the visible pulse was delayed after the infrared pulse, then the large nonresonant signal arising from a gold surface coated with ODT could be suppressed.¹² This suppression led to resonant peaks being much better resolved than in previous spectra in which the nonresonant signal from the gold surface was not suppressed.

In Lagutchev's work, they used an ultra fast broadband laser (~130 femtosecond pulse duration), which was split to produce a temporally asymmetric narrowband visible pulse and a broadband infrared pulse. When these two pulses were overlapped temporally and spatially, they combined to produce a VR-SFG spectrum of the ODT SAM's on gold. These spectra show both broad nonresonant response from the gold and narrow resonant response from the C18 chains. When the visible pulse was delayed to arrive after the infrared pulse, the nonresonant signal was eliminated completely from the resultant SFG spectra. However, the resonant signal arising from the surface bonded ODT chains has much longer lifetime. This longer lifetime allowed for the visible pulse to interact with the vibrationally excited molecules within the mode lifetime to produce a resonant-only VR-SFG spectrum.

Figure 1.9 illustrates this principle of a short-lived nonresonant signal and a longer lived vibrational resonance. This figure also shows the free induction decay of the resonant signal and the asymmetric visible pulse interacting with the resonant and nonresonant portions of the free induction decay. Because the nonresonant decay is virtually instantaneous, delaying the visible pulse eliminates the nonresonant signal from the overall VR-SFG spectrum.

Figure 1.9 also shows how cutting out, or apodizing, the beginning of the free induction decay not only eliminates the nonresonant signal, but the delay also cuts out the initial portion of the resonant free induction decay. Unfortunately, if we apodize the combined resonant/nonresonant free induction decay, we also apodize the resonant time domain spectrum. This apodized resonant time domain response does not contain all the information we would need to determine the actual frequency domain spectrum, and we realize that eliminates our ability to determine the absolute orientation of the surface molecules. The interference of resonant and nonresonant signals is unfortunate because we cannot separate the two signals easily.

Even with this resonant/nonresonant interference, VR-SFG spectra can still be used to obtain information about how the RPLC structure might change. If we delay the visible pulse after the IR, we can probe the resonant signal independent from the nonresonant signal, and determine if this resonant signal is changing in response to experimental conditions. Doing this eliminates our ability to say what the absolute orientation is, but we avoid the corrupting nonresonant signal contribution to our VR-SFG spectra. This technique of nonresonant suppression is relatively new, and its use is only possible if the two input pulses have a pulse duration on the same time scale as the resonant free induction decay.

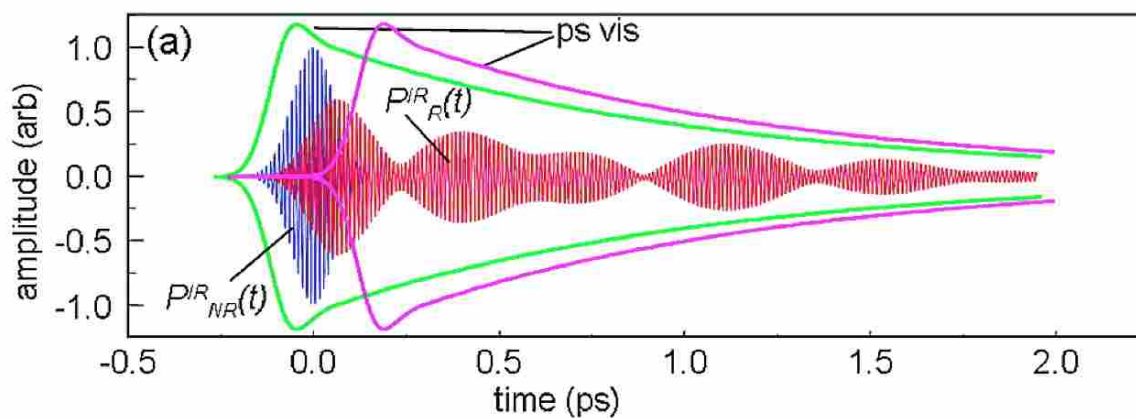


Figure 1.9. Resonant and nonresonant free induction decays as a function of time. The technique of time delay SFG is based on nonresonant background suppression developed by Laguchtev et al.¹² By delaying the visible pulse until after the fast decaying nonresonant signal has decayed substantially, we can probe the resonant-only free induction decay. Various times after the free induction decay allow resonant modes of different lifetimes and phases to be examined.

Reproduced with permission from publisher.

1.11 VR-SFG: Past RPLC Studies

Several researchers in this past decade have realized the potential that VR-SFG has when examining the stationary phase structure of the RPLC interface. Work at Brigham Young University that preceded mine has been invaluable. Those readers seeking an in-depth understanding of past work with VR-SFG and the model RPLC system are recommended to the graduate work of Brent Horn and Robert Baker, which has been an excellent source of knowledge for me.^{13,14} Of the published literature available, Marie Messmer's group at Lehigh University did extensive ambient pressure work aimed towards understanding the stationary phase structure with SFG.¹⁵⁻²⁰ It would be difficult and unnecessary to review all of the work that has been done with the RPLC system probed by VR-SFG. However, a brief introduction is important background for present and future work with the model RPLC system.

Figure 1.10 displays VR-SFG spectra from mixed polymeric C18/C1 stationary phases coated onto fused silica slides with different monolayer surface coverages.¹⁵ We examine here the denser coated $8.0 \mu\text{mol}/\text{m}^2$ surface coverage, which is more typical of the work that will be discussed in later chapters, and which represents polymeric C18. When this monolayer is exposed to air, they observed two prominent peaks at $\sim 2945 \text{ cm}^{-1}$ and $\sim 2878 \text{ cm}^{-1}$, which are identified as r^+ and a vaguely defined Fermi mode. These two peaks in the *ssp* polarization combination are typical for well ordered all trans polymeric C18 interfaces.²¹ When these stationary phases were exposed to acetonitrile or water, they observed a change in relative intensities of the two peaks and increased presence of the r^- mode at $\sim 2955 \text{ cm}^{-1}$, indicating the reorientation of the stationary phase in the solvents vs. exposure to air. However, there seems to be no effect by either acetonitrile or water to dramatically change the stationary phase structure with different solvents.

The presence of a great deal of order in these polymeric C18 stationary phases would seem to indicate that the alkyl chains do not simply collapse when placed in contact with solvents. From this study at ambient pressures, we can conclude that solute molecules encountering this interface would not “see” a collapsed “spaghetti” of C18 chains, but instead a well ordered system that has well packed all trans alkyl chains at a slight tilt from the surface normal. If the system had been greatly disordered, the VR-SFG signal would have been weak with a possibility of strong methylene modes present.

Messmer’s group could not have suppressed the nonresonant signal that may have interfered with their resonant signal interpretations. It is not immediately clear that their interpretations of the VR-SFG spectra were incorrect. More appropriately stated, the presence of nonresonant interference in the spectra they collected is possible and, by inference, the ability to assign absolute orientation for the RPLC stationary phase may be suspect. However, any spectral changes, however subtle, are likely an indication that the RPLC interface was changing in some way.¹⁵

This early work with the RPLC interface occurred a decade ago and is very helpful for determining the influence of ambient pressure solvent systems on the stationary phase at the RPLC interface. However, more work is needed to examine how this model chromatographic system responds to more relevant LC conditions, including elevated pressures. Using VR-SFG, we will attempt to properly examine the model RPLC interface exposed to typical RPLC conditions, such as elevated pressure with different mobile phases.

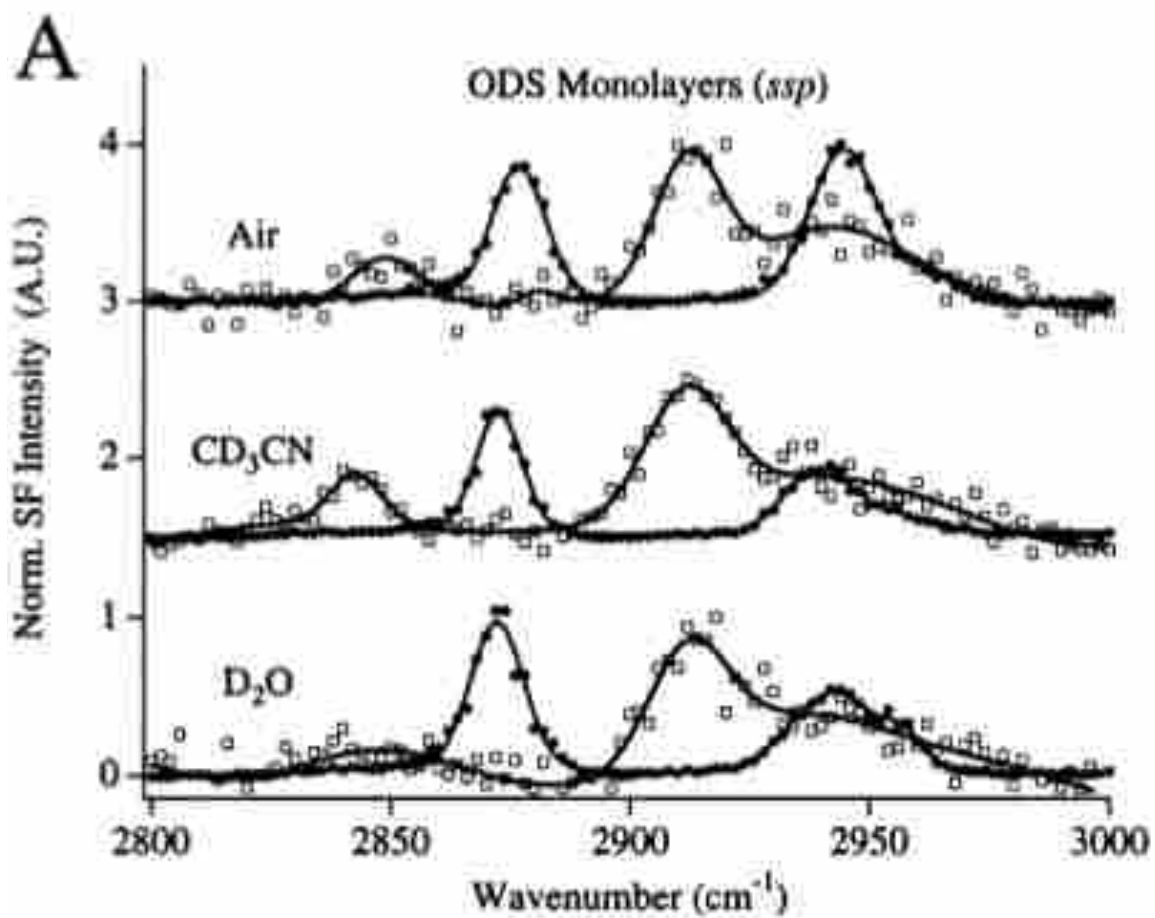


Figure 1.10 VR-SFG spectra of polymeric C18 monolayers coated onto fused silica examined under air, d-3 acetonitrile, and d-2 water.¹⁵ (•) indicates a surface coverage of $8.0 \mu\text{mol}/\text{m}^2$ and (□) indicates surface coverage of $4.5 \mu\text{mol}/\text{m}^2$. Reproduced with permission from publisher.

1.12 VR-SFG: Present Work

Figure 1.11 is a representation of the current set-up used to obtain VR-SFG spectra. Our VR-SFG system is based on an ultrafast (130 femtosecond pulse duration), high power (~2.7 Watts average power) Ti:sapphire laser (Integra from Quantronix lasers).²² A more in-depth description of this set-up is given in Chapter 3. Briefly, a broadband 790 nm laser with a repetition rate of 1 kilohertz is split into two beams. One beam is directed into a pair of Fabry-Pérot etalons that spectrally narrow the 790 nm beam and produce a temporally asymmetric visible pulse. The other portion of the original beam is used to pump an optical parametric amplifier (OPA), which converts the 790 nm light to a tunable broadband infrared beam centered at 2900 cm^{-1} . These two beams are temporally and spatially overlapped onto our samples, and the VR-SFG beam produced is directed into a monochromator and a CCD for detection.

We sought to improve the current understanding of model RPLC stationary phases. Using VR-SFG, we can probe this interface under *in situ* conditions typical of RPLC separations. Most importantly, we sought to understand if the stationary phase structure changed dramatically when exposed to elevated pressures. Before we could do this work, we had several problems to resolve. To properly interpret VR-SFG spectra, vibrational mode assignments must be properly made. Additionally, observed peak intensities must be corrected to yield actual peak intensities. Additionally, resonant/nonresonant interference must be properly understood. To accomplish these goals a variety of experiments were carried out.

Current literature assignments of the various C18 modes are at times vague and confusing. We have improved these mode assignments using isotopic substitution experiments with the typical RPLC stationary phases, octadecyltrichlorosilane (OTS) and chlorodimethyloctadecylsilane (ODMS). Isotopic substitution of the terminal methyl group was

necessary to separate the methyl modes from the methylene modes because they overlapped in the spectra. Using data from Fourier transform infrared spectroscopy, density functional theory calculations, and time delay VR-SFG, the five common peaks that we observe in our sample spectra were identified.^{23,12}

The second step in properly interpreting VR-SFG spectra was to intensity correct the spectra. The intensities of the different observed modes in our VR-SFG are not the actual intensities because the IR intensity profile is not the same over the entire output frequency range. These intensities must be corrected with the actual broadband IR intensity profile. To correct relative peak intensities, the actual IR intensity profile used in our VR-SFG experiments had to be determined. This was done using home-made gold mirrors that essentially up-convert the IR pulse through the SFG process.²⁴ Because these mirrors have a nonresonant-only response, the resultant spectra can be used to determine the actual IR intensity profile for each experiment. Once the sample spectra were intensity corrected, the actual resonant mode frequencies and identities were determined.

We were then able to understand structural information and determine the influence that the resonant/nonresonant interference has on our model RPLC interfaces. Investigation of our VR-SFG spectra at different delay times resulted in a better understanding of how to deal with the very real contributions that the nonresonant background has with the resonant molecular modes in our samples.

These experiments and their conclusions are described in subsequent chapters, and they will hopefully provide researchers with a better foundation for future work to understand the molecular basis for retention in model RPLC systems using VR-SFG. An improved understanding of the RPLC stationary phase and its structural changes in response to

experimental conditions may allow chromatographers to make more informed decisions on how best to perform separations. This knowledge-based approach will hopefully increase efficiency and make separations more of a science than an art.

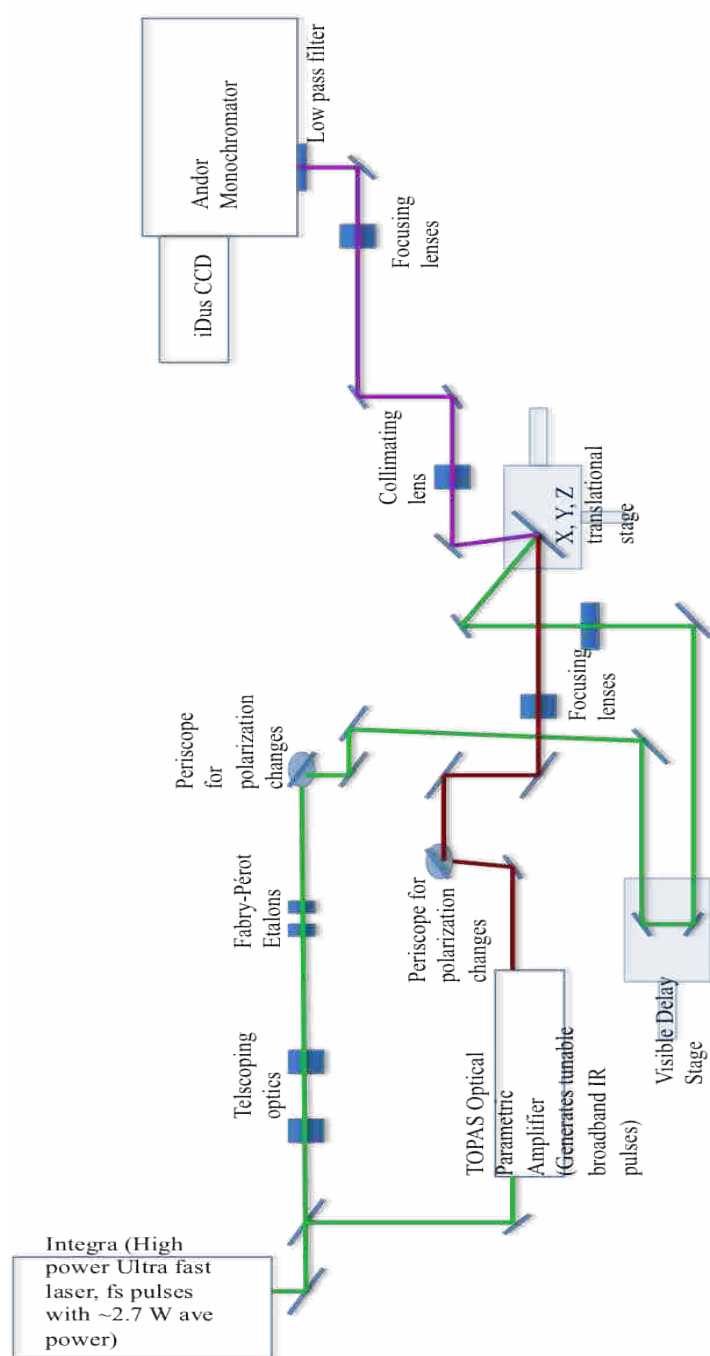


Figure 1.11. The VR-SFG set-up used in model RPLC experiments with a visible delay stage that allows for time delayed VR-SFG spectra.

1.13 References

1. J.G. Dorsey, K.A. Dill, *Chem. Rev.* 89 (1989) 331.
2. G.A. Howard, A.J.P. Martin, *Biochem. J.* 46 (1950) 532.
3. K.A. Dill, *J. Phys. Chem.* 91 (1987) 1980.
4. M.W. Ducey, C.J. Orendorff, J.E. Pemberton, L.C. Sander, *Anal. Chem.* 74 (2002) 5576.
5. M.W. Ducey, C.J. Orendorff, J.E. Pemberton, L.C. Sander, *Anal. Chem.* 74 (2002) 5585.
6. G. Srinivasan, L.C. Sander, K. Muller, *Anal. Bioanal. Chem.* 384 (2006) 514.
7. Y.R. Shen, *Nature* 337 (1989) 519.
8. C.D. Bain, *J. Chem. Soc., Faraday Trans.* 91 (1995) 1281.
9. J.C. Conboy, M.A. Kriech, *Anal. Chim. Acta* 496 (2003) 143.
10. T.T. Nguyen, K. Rembert, J.C. Conboy, *J. Am. Chem. Soc.* 131 (2009) 1401.
11. J.E. Patterson, A. Lagutchev, W. Huang, D.D. Dlott, *Phys. Rev. Lett.* 94 (2005) 4.
12. A. Lagutchev, S.A. Hambir, D.D. Dlott, *J. Phys. Chem. C* 111 (2007) 13645.
13. B.A. Horn, *Dissertation: Spectroscopic Investigations Of Chromatographic Processes*, Brigham Young University, Provo, UT, 2001.
14. L.R. Baker, *Thesis: Spectroscopic Study Of Compressible Mobile Phase And Stationary Phase Behavior In Chromatography*, Brigham Young University, Provo, UT, 2007.
15. M.C. Henry, L.K. Wolf, M.C. Messmer, *J. Phys. Chem. B* 107 (2003) 2765.
16. M.C. Henry, E.A. Piagessi, J.C. Zesotarski, M.C. Messmer, *Langmuir* 21 (2005) 6521.
17. X.Q. Li, M.C. Messmer, *J. Chromat., A* 984 (2003) 19.
18. Y. Liu, L.K. Wolf, M.C. Messmer, *Langmuir* 17 (2001) 4329.
19. Y. Liu, L.K. Wolf, M.C. Messmer, *Abs. Am. Chem. Soc.* 221 (2001) U378.
20. R.L. Pizzolatto, Y.J. Yang, L.K. Wolf, M.C. Messmer, *Anal. Chim. Acta* 397 (1999) 81.

21. B.C. Chow, T.T. Ehler, T.E. Furtak, *Appl. Phys. B: Lasers Opt.* 74 (2002) 395.
22. L.J. Richter, T.P. Petrali-Mallow, J.C. Stephenson, *Opt. Lett.* 23 (1998) 1594.
23. A.D. Curtis, S.B. Reynolds, A.R. Calchera, J.E. Patterson, *J. Phys. Chem. Lett.* 1 (2010) 2435.
24. A.D. Quast, F. Zhang, M.R. Linford, J.E. Patterson, *Appl. Spectrosc.* 65 (2011) 634.

Chapter 2

Improved Assignment of Vibrational Modes for Surface-Bound Alkylsilanes

2.1 Background

Structural determination of the C18 stationary phase is obtained through comparison of relative peak amplitudes and areas in the resultant VR-SFG spectrum. In order to fit SFG spectra and properly assign vibrational peaks in the SFG spectra, it is necessary to properly assign the five vibrational modes that may be excited in this region. The possible vibrational modes are: the CH₂ symmetric stretch (d^+), CH₃ symmetric stretch (r^+), the CH₂ antisymmetric stretch (d^-), the Fermi resonance mode, and the CH₃ antisymmetric stretch (r^-).

The symmetric and antisymmetric modes are relatively easy to assign but assignment of the Fermi resonance mode has been difficult because of its more complex origins. Fermi mixing can only occur if the two modes that mix are of the same symmetry and have similar energies.¹ At first glance, the terminal methyl group of the C18 silanes would appear to be of C_{3v} symmetry. This would seem to indicate that only groups of C_{3v} symmetry could mix, meaning we should assign the Fermi mode to the symmetric stretch and bend.

However, the terminal methyl group is not isolated. This means that the molecule formally belongs to the C_s point group. With symmetry of C_s , the C18 silane can couple any of the modes because they are not completely orthogonal to each other. In other words, entirely isolated vibrational modes do not exist. This makes determining the mode assignments of this molecule more an issue of finding which vibration is the primary component of an observed mode.

In the literature, this Fermi mode is assigned to the Fermi resonance of CH₃ symmetric stretch with possibly a small contribution from CH₂ asymmetric stretch.² This is confusing, because this mode has otherwise been assigned to the CH₃ symmetric stretch and the overtone of the CH₃ symmetric bend.^{3,4} Both assignments cannot be correct, and a definitive assignment is necessary to understand the C18 chain structure.

In order to clear up this confusion, we have worked to produce a deuterio-substituted terminal methyl group of formula Cl₃SiC₁₈H₃₄D₃. By deuterating the methyl group, the methyl stretch frequencies will be red-shifted when examined by vibrational spectroscopy.⁵ If this shifting results in the absence of the Fermi peak in the C-D stretch region, it is a good indication that it was indeed coupled to the methylene stretch. However, if there are three active modes in the C-D region, then the Fermi modes are a coupling of a CH₃ stretch and the overtone of a CH₃ bend.

To supplement the experimental data, I performed density functional theory calculations on (OH)₃SiC₁₀H₁₈D₃ and CD₃I. These molecules were chosen because they provide insights into our C18 silane, while being small enough for cheap computations. The calculated energies for these molecules are not absolutely the same as those observed experimentally in vibrational spectra because of the overestimation in the energies that results from variational theory. These computations do however provide useful ordering of mode assignments.

2.2 Experimental and Computational Methods

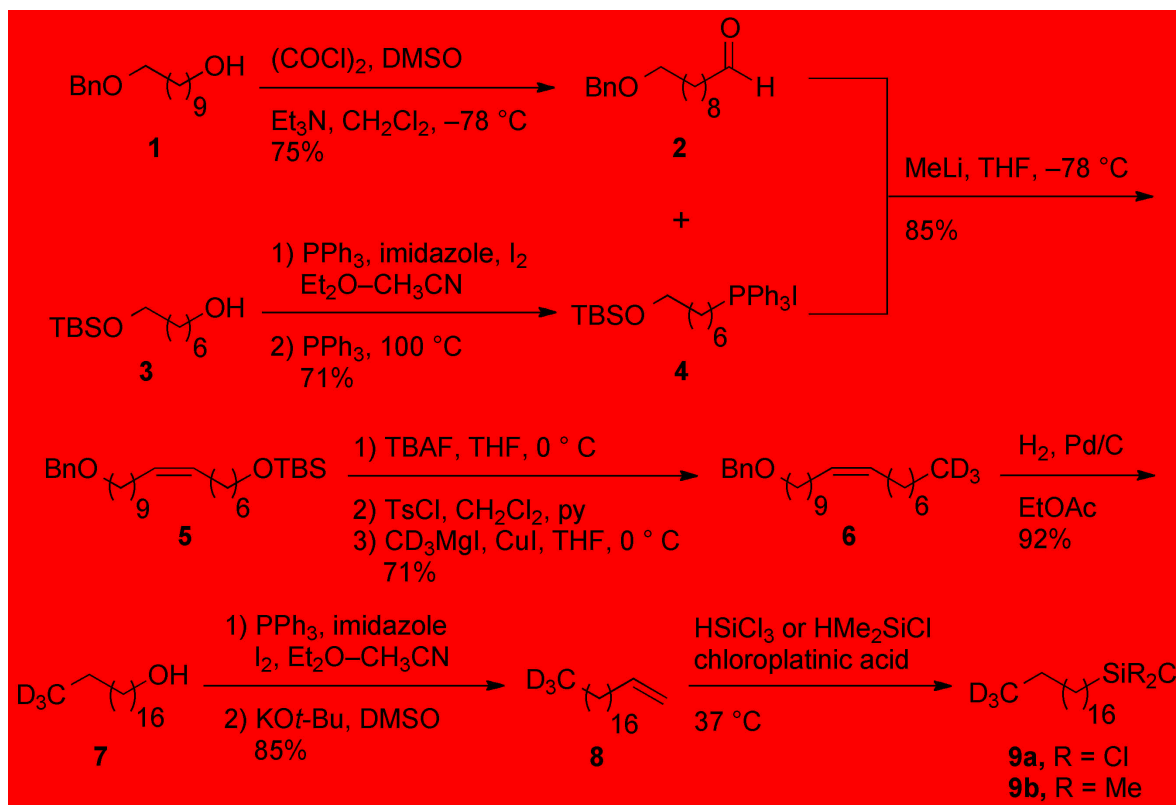
2.2.1 Synthesis of Deuterio-Substituted Molecules

Note: This work was highly collaborative. The Castle lab performed all of the organic synthesis, which is included here as a helpful reference to those interested in knowing exactly

how every part of this work was accomplished. I am very grateful for the Castle group's year of work that resulted in this synthesis.

Convergent synthesis of trichloro-(18,18,18-(trideuterio))-(octadecyl)silane was accomplished in a 10-step longest linear sequence from two commercially available monoprotected diols (Scheme 2.1). In this method 10-(benzyloxy)decan-1-ol **1** was converted to aldehyde **2** under Swern conditions.⁶ Also, 7-((*tert*-butyldimethylsilyl)oxy)heptan-1-ol **3** was subjected to Appel conditions⁷ to afford the iodide, and then converted to the corresponding Wittig salt **4**.⁷ Initial attempts to react **2** and **4** to yield alkene **5** were unsuccessful. We suspected that treating the salt with butyllithium was not affording the requisite ylide. We hypothesized that the large, nonpolar tail of our wittig salt caused it to form reverse micelles around water droplets, hindering the sterically bulky base from penetrating to deprotonate the phosphonium salt. We, therefore, elected to employ methyllithium, a much smaller base, and dry our wittig salt for 3 days in vacuo; using these conditions, we successfully synthesized alkene **5**.

Desilylation of **5**, with tosylate, and copper-promoted coupling⁸ with d_3 -methylmagnesium iodide afforded **6**, which was then hydrogenated to yield **7**. Our initial plan was to form another tosylate, and then eliminate to yield alkene **8**. However, our attempts were met with low yields and difficult separations. A literature search revealed that tosylates will undergo substitution with *tert*-butoxide to yield the *tert*-butyl ether.⁹ We therefore elected to convert the alcohol to an iodide instead, using Appel conditions. We then eliminated the subsequent iodide to yield alkene **8** with an 85% yield over two steps. This alkene was easily converted to silane **9** via hydrosilylation using trichlorosilane and chloroplatinic acid.¹⁰ Production of D_3 octadecyldimethylchlorosilane (D_3 ODMS) involved the use of dimethylchlorosilane (HMe_2SiCl) in the last step instead of trichlorosilane.



Scheme 2.1. Complete synthesis of monomeric and polymeric C18 silanes with a deuterated terminal methyl group.

2.2.2 Sample Preparation for Spectroscopic Characterization

2.2.2a FTIR Analysis

IR absorbance spectra were collected on a Nicolet 6700 FT-IR (Thermo Scientific) spectrometer with a resolution of 1 cm^{-1} and 164 scans. Neat spectra of five compounds were collected: $\text{D}_3\text{H}_{32}\text{C}_{18}$, $\text{D}_3\text{H}_{34}\text{C}_{18}\text{Cl}_3\text{Si}$, $\text{D}_3\text{H}_{34}\text{C}_{18}(\text{CH}_3)_2\text{ClSi}$, $\text{H}_{37}\text{C}_{18}\text{Cl}_3\text{Si}$, and $\text{H}_{37}\text{C}_{18}(\text{CH}_3)_2\text{ClSi}$. The neat compounds were placed on NaCl plates (1" round by 1/8" thick). Uncoated salt plates were used as our sample blanks.

2.2.2b VR-SFG Analysis

Trichloro(octadecyl)silane ($\geq 90\%$), water, acetone, and methanol were obtained from Sigma-Aldrich. Chloroform was obtained from EMD chemicals. Dichloromethane and sulfuric acid (technical 93%) were obtained from Mallinckrodt. Hydrogen peroxide (30%) was obtained from Fischer Scientific. All solvents were HPLC grade and used as received. Rinsing water was obtained from a ultrapure Millipore Milli-Q RG water system with a resistivity of $18\text{ M}\Omega\text{-cm}$. Fused silica discs of 1" diameter and 1/8" thickness were obtained from Quartz Scientific. The discs were sonicated in chloroform for ~ 1 min and then placed in 120°C *piranha* solution (3:1 sulfuric acid and hydrogen peroxide) for 1 h. (*Note: Piranha* solution is very corrosive and extreme care must be used when handling.) The discs were then rinsed with copious amounts of water, acetone, chloroform, and dichloromethane and placed in a beaker with 100 mL of dichloromethane. This cleaning procedure is required to remove any organic contamination that may confuse the spectroscopic measurements. A 1-mL of trichloro(octadecyl)silane (for polymeric OTS samples) was added to the solution before sealing in a nitrogen purged glove box and shaking for 24 h. The discs were then removed from the solution and immediately rinsed with copious amounts of dichloromethane, acetone, water, acetone, and chloroform, followed by

sonication for 1 min in chloroform. The discs were again rinsed with chloroform, acetone, water, acetone, and then stored in either methanol or ultrapure 18 M Ω water from a Millipore system. This procedure was based on work by Messmer and co-workers.² The octadecyldimethylsilane (ODMS) and dimethylsilane (DMS) samples were treated exactly as described above except that they were not immersed in a reaction solution. Instead fused silica flats were dried and sandwiched with a few drops of ODMS or DMS in between two flats. These flats were then placed on a hot plate heated to 100 °C and 25 °C for the ODMS and DMS samples, respectively, for 15 min.¹¹ The samples were then separated and cleaned as described above. All samples were stored in ultrapure water until use. A Ramé-hart model 100-00 goniometer was used to obtain water contact angles averaging $\sim 109^\circ$ and $\sim 101^\circ$ for OTS and ODMS surfaces, respectively.

2.2.3 VR-SFG System

Set-up and Instrumentation: The vibrationally resonant sum-frequency generation (VR-SFG) spectroscopy system is based on an amplified Ti:sapphire laser system (Quantronix, Integra C) that produces 3 mJ per pulse at 1 kHz. The pulse duration was ~ 130 fs. The beam is split, with the majority pumping a broad band IR optical parametric amplifier (Quantronix, TOPAS-C) to produce ~ 22 μ J with a bandwidth of 250 cm^{-1} IR light centered in the C-H stretch region, around 2900 cm^{-1} . A germanium filter removes any remaining visible light from the OPA. The remaining light passes through a Fabry-Pérot etalon to provide the spectrally narrow (10 cm^{-1}) visible pulse at 792 nm. Visible pulse energy was 20 μ J, with the visible beam defocused sufficiently to prevent damage to the sample. Polarization control of both the IR and visible beams is accomplished with periscopes. In all experiments, the IR beam was *p*-polarized, and the visible beam was *s*-polarized. This input combination only produces *s*-polarized SFG, which was rotated 90 ° by a half waveplate for optimal detection by the spectrometer (Andor

Shamrock) and CCD (Andor iDus). An optical filter was also placed before the spectrometer to remove any reflected or scattered visible light.

2.2.4 Computational Methods

Computations were performed using the NWChem 6.0 software package.¹² Optimized geometries and vibrational frequencies for CD₃I were determined with 32 functions in a LANL2DZ ECP basis set under renormalized density-functional theory (RDFT) with the density functional theory (DFT) combined function of a Becke, three-parameter, Lee-Yang-Parr (B3LYP) hybrid. Optimized (OH)₃SiC₁₀H₁₈D₃ geometry, and vibrational frequencies were obtained using 32 functions with a 6-31G* basis set under renormalized density-functional theory (RDFT) with the density functional theory (DFT) combined function of B3LYP hybrid.

2.3 Results and Discussion

2.3.1 FTIR Spectra

FTIR spectra of five different compounds were obtained: D₃H₃₂ alkene precursor, the two D₃ substituted silanes, D₃H₃₄ OTS and D₃H₄₀ ODMS, as well as the fully hydrogenated silanes, H₄₃ ODMS and H₃₇ OTS. Figure 2.1 shows the FTIR spectra of these five compounds in the CH stretch region.

2.3.1a CH Stretching Region

These spectra are dominated by CH₂ stretches because there are seventeen (for polymeric OTS) methylene units for each methyl unit, making the absorption by methylene units much more pronounced. These methylene stretches are easily identified from the D₃H₃₂ alkene shown in 2.1a because this molecule does not contain a CH₃ moiety. The lower energy mode is readily assigned to d⁺ at ~2850 cm⁻¹ and d⁻ at ~2920 cm⁻¹. Further confirmation of the D₃H₃₂ alkene is seen by the sp² peak at ~3076 cm⁻¹. Figure 2.1b displays the spectrum for D₃H₃₄ OTS, which

does not contain a CH₃ moiety and also lacks structure outside of the methylene modes. Figure 2.1c, d, e all have CH₃ moieties and show additional symmetric and antisymmetric modes on the blue side of the methylene modes.

2.3.1b CD Stretching Region

Inspection of these molecules in the CD stretch region is even more informative (Figure 2.2). The stretches from 2000-2300 cm⁻¹ can be attributed to CD stretches because the undeuterated compounds (Figure 2.2d, e) do not have any noticeable features in this range. We observe three modes in the D₃H₃₂ alkene (Figure 2.2a) which can again be assigned to the lower energy r⁺ at ~2073 cm⁻¹. And on the high energy side, we observe an asymmetric peak assigned to r⁻ at ~2210 cm⁻¹.

We also observe a peak in the D₃H₃₄ OTS spectrum at 2250 cm⁻¹, which also appears in trichlorosilane (Cl₃SiH) spectra. We, therefore, attribute this peak to the SiH stretch. Contamination of our D₃H₃₄ OTS compound with the polymerized trichlorosilane produces the broad feature that occurs at ~2250 cm⁻¹.¹³ The broadening in the Si-H peak is likely due to the polymerization of the trichlorosilane. The Si-H environment is varied and different enough to yield many different modes, which leads to a smearing out of these peaks in the condensed phase.

The absence of the Si-H peak in the D₃ ODMS is further evidence of the contaminated product, because the synthesis for the D₃ ODMS reagent concludes with the addition of dimethylchlorosilane to D₃ octadecene. Even though the dimethylchlorosilane contains an Si-H bond, it is less likely to appear in FTIR spectra. This is because the final hydrolyzed monomeric silane can only dimerize. This would leave leftover dimethylchlorosilane to be rinsed away with

cleaning of the final product before making the neat film FTIR samples, and we would not see Si-H peaks in the ODMS samples.

2.3.1c Fingerprint Region

The fingerprint region for these molecules is shown in Figure 2.3. Although this region is rich in information, we only highlight a few features. The CD₃ bending is observed around ~1050 cm⁻¹ only in the deuterated compounds. The peak at 1235 cm⁻¹ is attributed to the CH₃ symmetric bending mode attached to the silicon atom at the base of the C18 chain.¹⁴ The CH₃ bending occurs just below 1500 cm⁻¹, with the methylene bending modes making it difficult to identify.

2.3.2 DFT Calculations

Density functional theory calculations help to further identify the CD₃ stretching modes. It should be noted that the actual frequencies are too high, but the order of energies for the different modes is correct. Because DFT is a variational approach, the calculated energies must be greater than or equal to the real energy.

Table 2.1 shows DFT calculations for two molecules, D₃H₁₈C₁₀Si(OH)₃ and CD₃I. From these calculations, we can identify some general trends for molecules with a CD₃ moiety. The bending modes occur at energies of about half that of the stretch modes. The doubly degenerate antisymmetric methyl stretch has a wider spacing between the two degenerate methyl antisymmetric stretches in the long chain silane vs. the close spacing of the degenerate modes in the D₃ iodomethane.

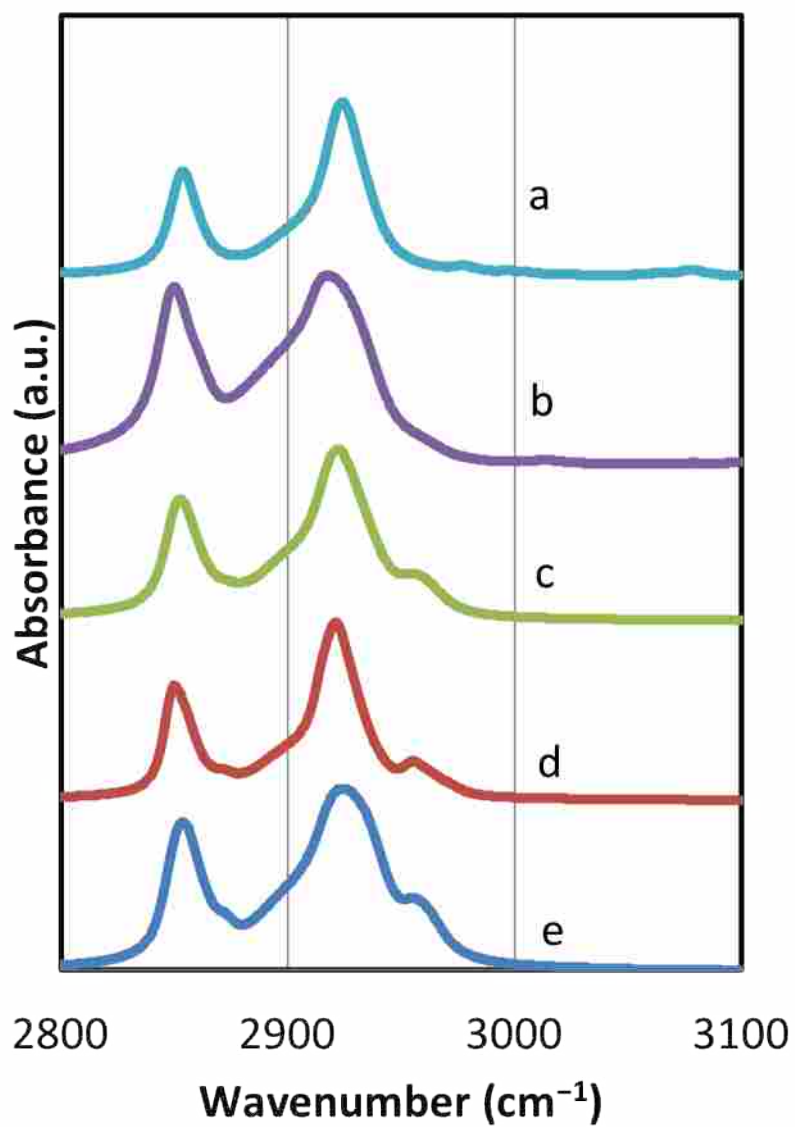


Figure 2.1. FTIR Spectra in the CH Stretching region. Note the sp^2 peak at $\sim 3076\text{ cm}^{-1}$ in the alkene precursor. (a) D_3H_{32} Alkene (b) D_3H_{34} OTS (c) D_3H_{40} ODMS (d) H_{43} ODMS (e) H_{37} OTS.

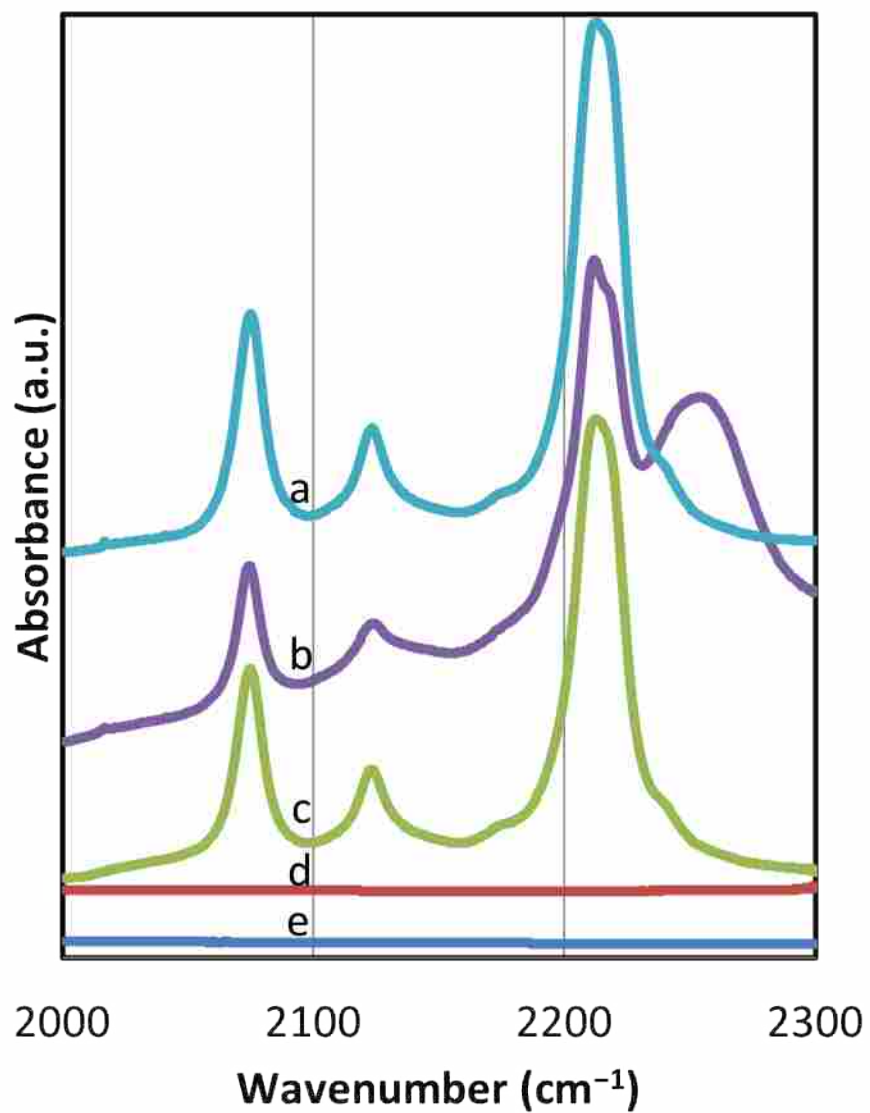


Figure 2.2. FTIR Spectra in the CD Stretching region. (a) D₃H₃₂ Alkene (b) D₃H₃₄ OTS (c) D₃H₄₀ ODMS (d) H₄₃ ODMS (e) H₃₇ OTS.

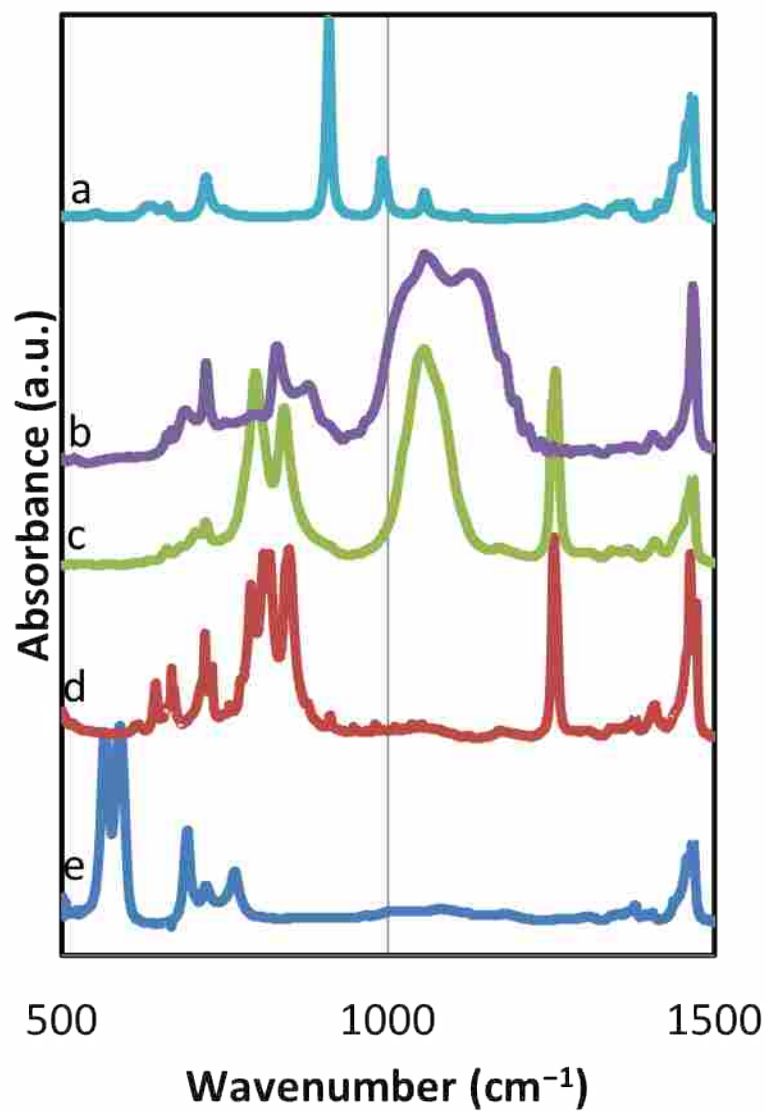


Figure 2.3. FTIR Spectra in the fingerprint region. (a) D₃H₃₂ Alkene (b) D₃H₃₄ OTS (c) D₃H₄₀ ODMS (d) H₄₃ ODMS (e) H₃₇ OTS.

Table 2.1. Peak assignments of C10 D3 silane and CD₃I from calculations. The order of peak assignments in the table corresponds to similar trends in FTIR data for the D3 containing molecules.

	DFT Data	
	C10 D ₃ silane (cm ⁻¹)	CD ₃ I (cm ⁻¹)
Symm methyl bend	1160	993
Asymm methyl bend (g _j =2)	1104	1082
	1100	1082
Symm methyl stretch	2185	2221
Asymm methyl stretch (g _j =2)	2297	2396
	2304	2396

2.3.3 VR-SFG Spectra: *ssp* vs. *sps*

Figure 2.4 shows the VR-SFG spectra of H₃₇ OTS in two polarization combinations in the CH stretch region. The densely packed silane on a fused silica flat has two sharp peaks in the *ssp* combination at $\sim 2880\text{ cm}^{-1}$ and $\sim 2950\text{ cm}^{-1}$, which are commonly assigned to the symmetric methyl stretch and the “Fermi mode.” However, the *sps* polarization combination only shows one peak at $\sim 2960\text{ cm}^{-1}$, usually attributed to the antisymmetric stretch of the terminal methyl group.⁴

2.3.4 Variable Time Delay VR-SFG Spectra: *ssp*

Delaying the visible pulse at various intervals after the IR pulse allows us to probe different parts of the resonant free induction decay. By examining the free induction decay at different points, we can see changes in relative intensities of the peaks. These changes are a result of the different vibrational mode lifetimes and phases. In Figure 2.5, the spectrum at optimal pulse overlap is highly convoluted by overlapping peaks. Careful examination of Figures 2.4 and 2.5 show at least 5 peaks.^{15,16} From low to high energy, these modes occur at about: 2860 cm^{-1} , 2884 cm^{-1} , 2930 cm^{-1} , 2950 cm^{-1} , and 2963 cm^{-1} . Figures 2.4 and 2.5 are more than adequate for identifying these 5 peaks.

2.3.5 VR-SFG of ODMS and DMS

Figure 2.6 shows the VR-SFG spectra of ODMS and DMS. The spectrum of ODMS is very complicated and it is difficult to identify well-resolved peaks. The C18 chain in the ODMS molecule should have the same 5 peaks observed for the OTS spectrum with the addition of basal methyl groups. Examining the DMS spectrum can identify these basal methyl groups. We expect the basal methyl groups to have a symmetric stretch, a possible Fermi mode, and an antisymmetric stretch.

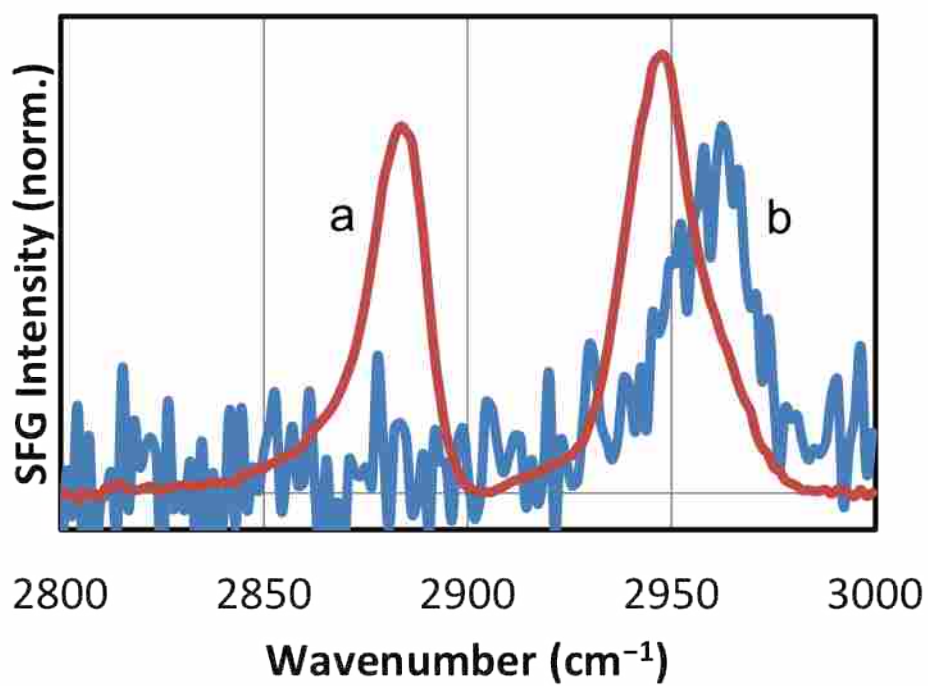


Figure 2.4. VR-SFG spectra in the CH Stretching region with the sample exposed to air. (a) *ssp* combination H₃₇ OTS, (b) *sps* combination H₃₇ OTS.

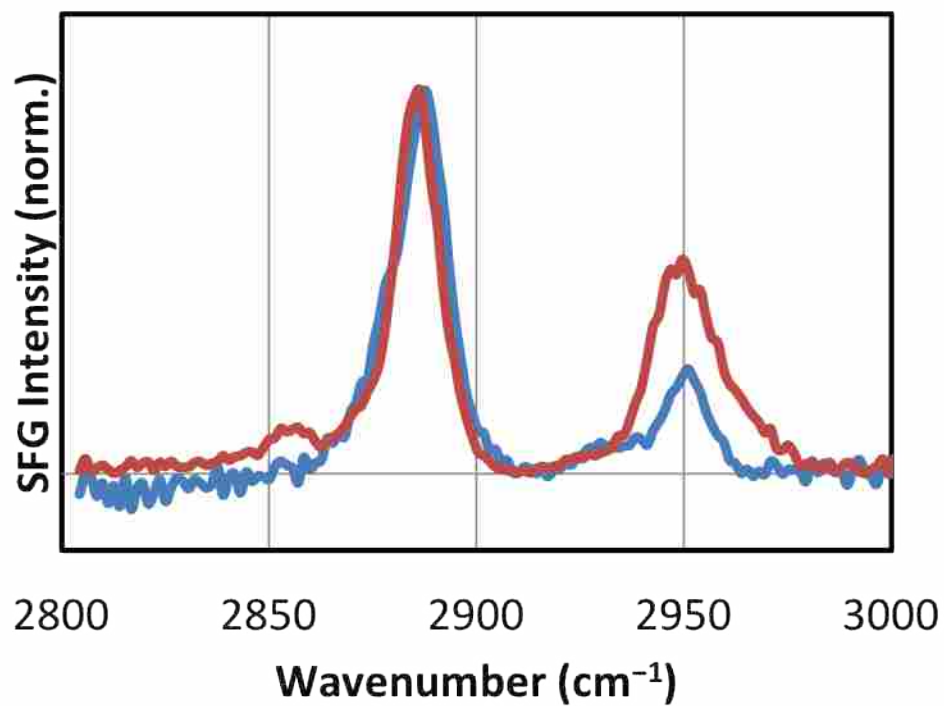


Figure 2.5. Time delayed spectra showing 5 peaks that are identified in an H₃₇ OTS spectrum. (Red) *ssp* 0 s delay exposed to solvent, (Blue) *ssp* 2.54 ps delay exposed to air.

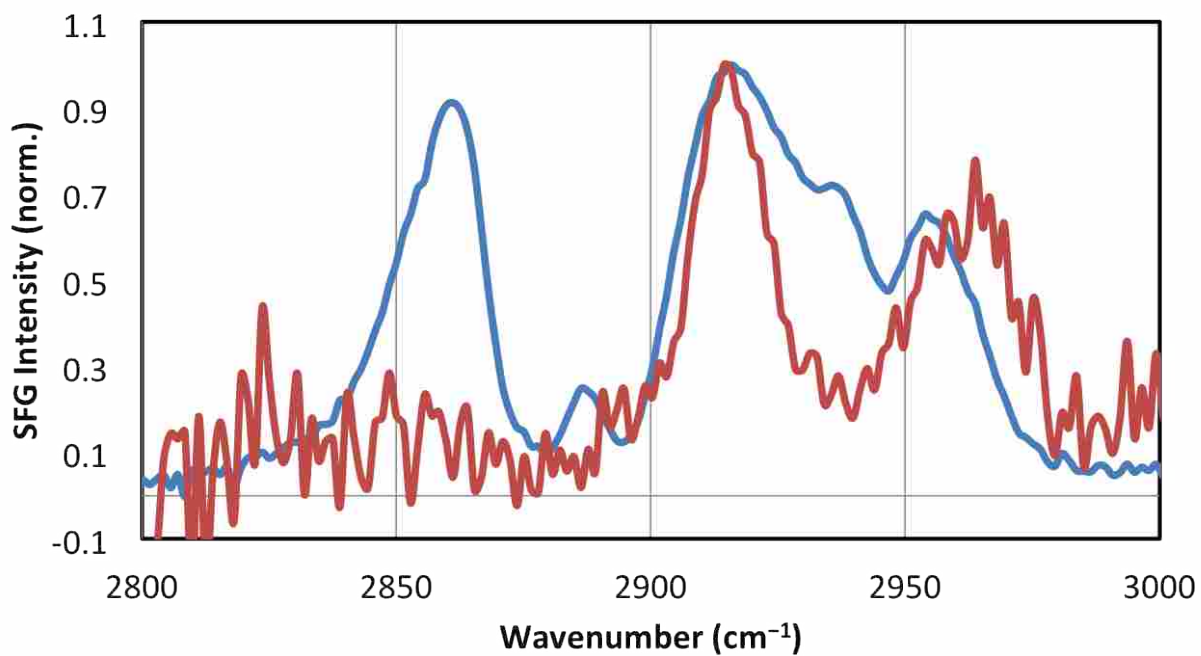


Figure 2.6. VR-SFG of silanes on fused silica in the *ssp* polarization combination. (Red) Chlorodimethylsilane; (Blue) ODMS.

2.4 Additional Discussion and Conclusions

Using information obtained through FTIR spectroscopy, DFT calculations and different polarization combinations of VR-SFG, we were able to logically assign the CH stretches in a typical VR-SFG spectrum of C18 silanes on fused silica flats. The symmetric modes occur at lower energies than the antisymmetric modes for both methyl and methylene groups (See DFT calculations). We are also confident about the relative position of the methylene modes, which are lower in energy than the methyl modes.

Unfortunately, the presence of the Fermi mode leads many researchers to believe that it can arise from apparently several combinations of modes. Although this assumption is not stated explicitly in the literature, different research groups assign the same peak to different combinations, leading us to assume that no absolute identification of the source of the Fermi mode has been made.^{4, 17}

The C18 silane symmetry is reduced to the C_s point group. With C_s symmetry, any two modes could interact in a Fermi fashion if the energies match. In fact, as we work to identify the Fermi mode in the C18 silane, it should be noted that its presence is not likely only from the interaction of two modes. More correctly stated, the Fermi mode may be a combination of all the vibrational modes of similar energies in the C_s molecule. However, we can identify the major contributors to the Fermi mode.

Using the FTIR data from the D3 substituted silanes made in house, we are able to definitively state that the Fermi mode does not arise from a combination of the methylene and the methyl modes. This is because the CD region of the deuterio-substituted molecules contains three peaks, not only two. The asymmetric lineshape of one of these peaks identifies it as the

doubly degenerate antisymmetric methyl stretch, which is split in the long chain silane. The low energy symmetric stretch is also seen with the addition of a third peak in between the two stretches. This additional peak must be the Fermi mode, and its presence in the deuterio-substituted molecule means that it cannot be a coupling of the methyl modes with the methylene modes. The isotopic substitution should eliminate the Fermi mode if it were due to the methyl and methylene modes.

We also note that the Fermi mode occurs at about the same frequency as the doubled methyl bend modes. This is confirmed in the fingerprint region of the D3 substituted molecules as well as the DFT calculations. From these two observations, we can now identify the source of the Fermi mode to be the coupling of the methyl stretch with the overtone of the methyl bend.

However, is this due to the combination of symmetric bend with antisymmetric stretch, symmetric stretch with symmetric bend, or antisymmetric bend with antisymmetric stretch? To answer this question, a densely packed H₃₇ OTS coated fused silica flat was investigated with different polarization combinations of VR-SFG. Densely packed C18 OTS SAM's have two sharp peaks in the CH stretch region in air under the *ssp* combination. Both peaks are equally intense and were identified as the symmetric methyl stretch and the Fermi mode. In the densely packed phase, we expect that the terminal methyl group would have a net tilt, relative to the surface normal, close to 0°. The lack of prominent methylene modes indicates an all-trans configuration.

In a polarization combination with the electric field of the IR pulse parallel to the plane of incidence, we would expect the symmetric methyl stretch and bend to be excited. A polarization combination perpendicular to the plane of incidence would then excite the antisymmetric methyl stretch and bend. Indeed we observe two sharp peaks in the *ssp* combination, and those two

peaks disappear in the *sps* combination, leaving only a very weak methyl antisymmetric stretch to be observed. Because we see this loss of the Fermi mode in the *sps* combination, we can say with reasonable certainty that this mode is due to the symmetric stretch with the overtone of the symmetric bend.

We also note that the methyl symmetric stretch and the Fermi mode for orientational analysis are of limited usefulness because these two peak amplitudes are actually a mixing of the methyl symmetric stretch with the overtone of the methyl symmetric bend. As these two states mix they “borrow” intensity from each other meaning the weaker mode is amplified and the stronger mode is attenuated. This intensity borrowing corrupts the true intensities and reduces our confidence in determining molecular orientation.

After numerous DFT calculations and experiments using FTIR and SFG, we have assigned the C-H stretching region of C18 polymeric and monomeric silanes. The Fermi mode that occurs at $\sim 2124\text{ cm}^{-1}$ is attributed to the coupling of the methyl symmetric bend overtone with the methyl symmetric stretch. Using the data from SFG and FTIR we can now assign all the observed modes in the C-H stretch region to be the symmetric/antisymmetric methyl/methylene modes (4 modes) and the Fermi resonance mode. Figure 2.7 is a reproduction of Figure 2.5 and is included as a reference to identify the various modes present in VR-SFG spectra of the polymeric C18 stationary phase. Using the identified peaks from the OTS spectra and the additional information from the DMS spectrum we can also identify the likely vibrational modes present in a VR-SFG spectrum of ODMS molecules (Figure 2.8). This proper assignment eliminates the ambiguity of these peak assignments for these C18 silanes as well as eliminates the confusion with long chain alkanes having similar moieties.

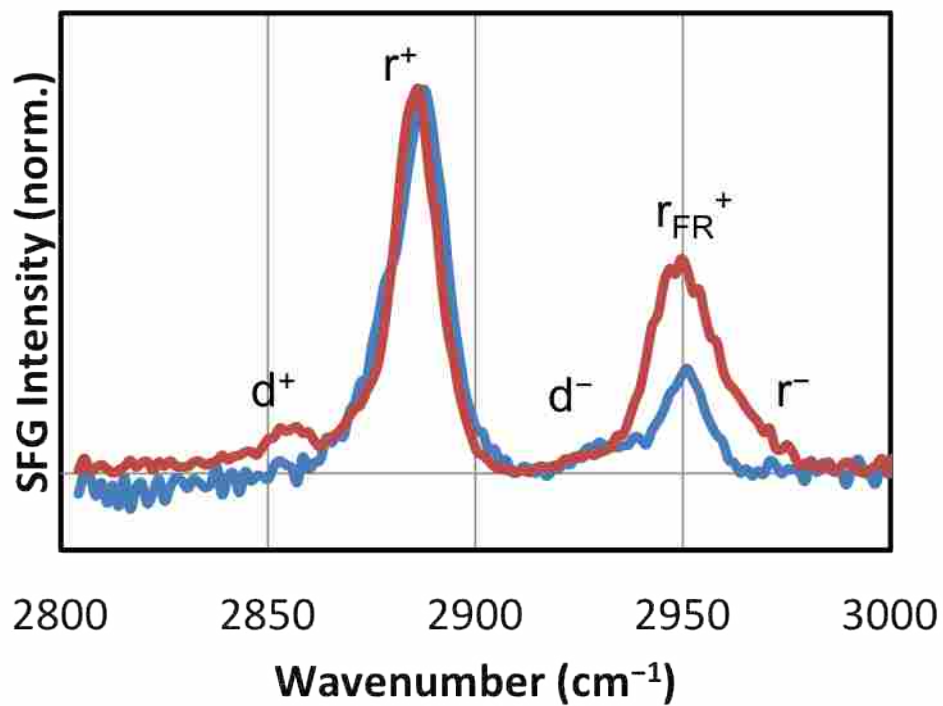


Figure 2.7. Reproduced Figure 2.5 with the five observed modes labeled. Time delayed spectra showing 5 peaks that are identified in an H₃₇ OTS spectrum. (Red) *ssp* 0 ps delay exposed to solvent, (Blue) *ssp* 1.27 ps delay exposed to air.

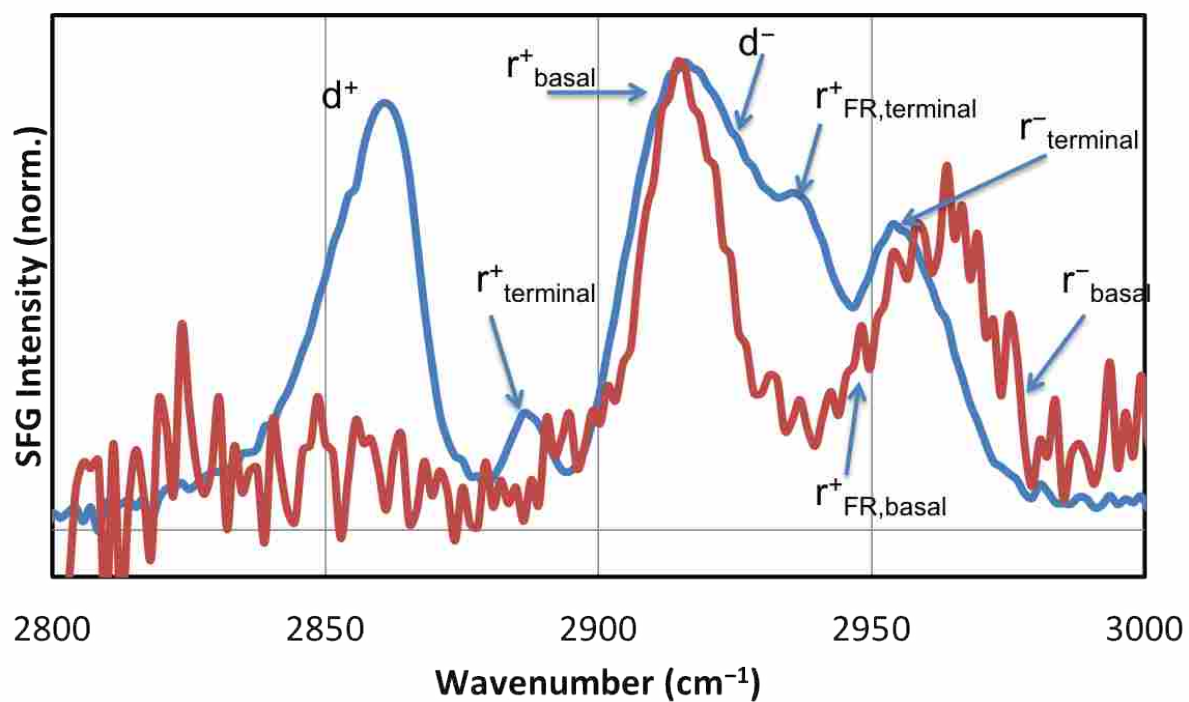


Figure 2.8. VR-SFG of silanes on fused silica in the *ssp* polarization combination. (Red) Chlorodimethylsilane; (Blue) ODMS.

2.5 References

1. J.L. McHale, *Molecular Spectroscopy*. Printice-Hall: Upper Saddle River, NJ, 1 (1999).
2. Y. Liu, L.K. Wolf, M.C. Messmer, *Langmuir* 17 (2001) 4329.
3. J.E. Patterson, A. Lagutchev, W. Huang, D.D. Dlott, *Phys. Rev. Lett.* 94 (2005) 4.
4. B.C. Chow, T.T. Ehler, T.E. Furtak, *Appl. Phys. B: Lasers Opt.* 74 (2002) 395.
5. G. Ma, H.C. Allen, *J. Phys. Chem. B* 107 (2003) 6343.
6. T. Muller, D. Coowar, M. Hanbali, P. Heuschling, B. Luu, *Tetrahedron* 62 (2006) 12025.
7. Y. Kita, T. Toma, T. Kan, T. Fukuyama, *Org. Lett.* 10 (2008) 3251.
8. J.R. Vyvyan, C.L. Holst, A.J. Johnson, C.M. Schwenk, *J. Org. Chem.* 67 (2002) 2263.
9. N.F. Wood, F.C. Chang, *J. Org. Chem.* 30 (1965) 2054.
10. P. Savage, Ph.D. Dissertation, The University of Wisconsin, 1993.
11. G.A. Hussein, J. Peacock, A. Sathyapalan, L.W. Zilch, M.C. Asplund, E.T. Sevy, M.R. Linford, *Langmuir* 19 (2003) 5169.
12. M. Valiev, E.J. Bylaska, N. Govind, K. Kowalski, T.P. Straatsma, H.J.J. Van Dam, D. Wang, J. Nieplocha, E. Apra, T.L. Windus, W. De Jong, *Comput. Phys. Commun.* 181 (2010) 1477.
13. T. Shimanouchi, *J. Phys. Chem. Ref. Data* 6 (1972) 993.
14. A. Fidelis, F. Ozanam, J.N. Chazalviel, *Surface. Surf. Sci.* 444 (2000) L7.
15. A. Lagutchev, S.A. Hambir, D.D. Dlott, *J. Phys. Chem. C* 111 (2007) 13645.
16. A.D. Curtis, S.B. Reynolds, A.R. Calchera, J.E. Patterson, *J. Phys. Chem. Lett.* 1 (2010) 2435.
17. M.C. Henry, L.K. Wolf, M.C. Messmer, *J. Phys. Chem. B* 107 (2003) 2765.

Chapter 3

Back-Surface Gold Mirrors for Vibrationally Resonant Sum-Frequency (VR-SFG) Spectroscopy Using 3-Mercaptopropyltrimethoxysilane as an Adhesion Promoter

Note: This work was published in the June 2011 issue of Applied Spectroscopy.¹ I would like to thank Feng Zhang for performing the work with principal components analysis, XPS, TOF-SIMS, ellipsometry, and goniometry. This paper, as published, represents an exhaustive analysis of back-surface gold reference mirrors for VR-SFG intensity correction. Permission from the publisher has been obtained to reprint this paper with minor modifications.

3.1 Introduction

Metal mirrors have a long history in spectroscopy, with gold, silver, and aluminum mirrors most commonly used. Commercial front-surface metal mirrors offer high reflectivity in the visible and the near infrared (NIR) portions of the spectrum; protected gold mirrors can have overall reflectivity of >90% in the 600 nm – 20 μ m range, making them useful deep into the IR. Not all spectroscopic applications can utilize front-surface mirrors, however. For example, for spectroscopic monitoring of a reaction chamber with multiple optical passes, conventional mirrors could be susceptible to corrosion or oxidation. In this case, back-surface mirrors would be more effective; the substrate would serve as a window to the chamber and also protect the mirror surface. Unfortunately, options for back-surface metal mirrors are limited because of the poor adhesion of these metals to silicon, fused silica, or BK7 substrates. For gold mirrors, a chromium, nickel, or titanium adhesion layer is typically applied between the gold and the substrate, which limits the usefulness of the mirror to its front surface; these other metals do not

have the desired reflectivity of gold or silver. The ability to make durable metal mirrors with no metal adhesion layer would allow for highly reflective front and back surfaces.

The applications of back-surface metal mirrors most relevant to our research are the *in situ* monitoring of reversed-phase liquid chromatography (RPLC) stationary phases and probing buried polymer interfaces. We use the nonlinear optical technique of vibrationally resonant sum-frequency generation (VR-SFG) spectroscopy in this effort.² VR-SFG allows one to obtain structural information from buried interfaces *in situ* under various experimental conditions. In this method, two laser beams are incident on the sample. The first is a narrow-band visible pulse and the second is a broadband IR pulse, centered in the CH stretch region at ca. 2900 cm^{-1} .³ The two beams mix at the interface, generating a third beam at the sum of the two incident frequencies. The selection rules of this process dictate that only molecules at the interface produce an SFG signal, where resonant enhancement with the vibrational modes of the molecules at the interface provides information about their structures.

Because our IR source is broadband, the measured intensity of each vibrational mode must be corrected for the IR intensity profile. The IR profile is typically obtained by upconversion with the visible pulse on a reference material, such as GaAs or a noble metal, commonly gold. Assuming that the reference material has a purely nonresonant response, the reference SFG spectrum can be used to intensity-correct subsequent spectra. When probing buried interfaces, it is advantageous to have the reference material in the same physical location as the interface being probed to account for all optical effects of the substrate or other materials. The ideal reference material for our applications is therefore a back-surface gold mirror.

Our work imposes three requirements for a reference mirror: it must have high back-surface reflectivity, be free of spectral interference, and be durable. Gold can be thermally

evaporated onto fused silica flats without a chromium adhesion layer, creating a back-surface mirror, but unfortunately these mirrors are not durable because of the poor adhesion of gold to the substrate. An adhesion layer of some kind is necessary to improve durability,^{4,5,6} but the layer must also cause little or no spectral interference. One candidate molecule is 3-mercaptopropyltrimethoxysilane (MCPTMS), a bifunctional silane that can bind to the fused silica substrate with the methoxy groups, leaving a thiol group for bonding with metals such as gold, silver, copper, or platinum.⁷ (See Figure 3.1) MCPTMS has been used for multiple applications, including gold film adhesion,⁸⁻¹⁷ and characterization of MCPTMS monolayers, with and without attached gold, suggests they will work well as a component of back-surface mirrors.¹⁸⁻²⁰ The main question to be addressed is whether the monolayer of MCPTMS between the substrate and the mirror surface will significantly affect the reflectivity of the metal in the spectral region of interest.

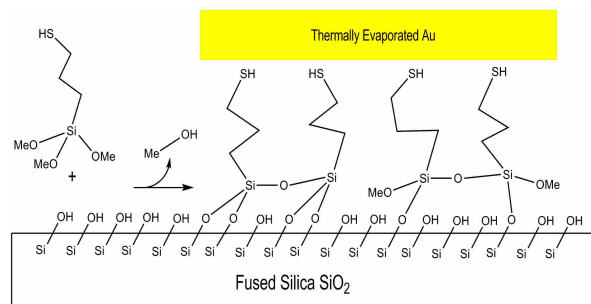


Figure 3.1. Schematic of the process to fabricate back-surface mirrors. Deposition of the MCPTMS onto a clean fused silica surface is followed by thermal deposition of gold.

In this paper, we describe the fabrication of durable back-surface gold mirrors with chemical vapor deposited 3-mercaptopropyltrimethoxysilane (MCPTMS) as a molecular adhesion layer. We also report spectroscopic characterization of the buried interface and demonstrate the usefulness of these mirrors as references for VR-SFG spectroscopy.

3.2 Experimental Methods

HPLC grade chloroform was obtained from EMD Chemicals (Gibbstown, NJ), sulfuric acid (technical, 93%) from Mallinckrodt (Phillipsburg, NJ), hydrogen peroxide (30%) from Fischer Scientific (Waltham, MA), and MCPTMS from Gelest (Morrisville, PA). All materials were used as received. Rinsing water was obtained from a Millipore Milli-Q RG water system with a resistivity of 18 M Ω -cm. Nitrogen was obtained from Airgas and used as received. Fused silica discs of 1" diameter and 1/8" thickness were purchased from Chemglass Life Sciences (Vineland, NJ). Single polished, 600 μ m thick silicon (100) pieces (Montco Silicon Technologies, Spring City, PA) were run in the same batches as the fused silica discs for detailed surface characterization.

The fused silica discs were sonicated in chloroform for ca. 1 min. To more fully clean the discs and generate free silanols for silane attachment, the discs were then immersed in 120 °C *piranha* solution (3:1 concentrated sulfuric acid and 30% hydrogen peroxide) for 2 h. (*Note: Piranha* solution is very corrosive and extreme care must be used when handling it. Organic matter may react explosively on contact with it.) The discs were then rinsed with copious amounts of water and stored in water. Before coating, the discs were dried under a stream of dry nitrogen. Coating with MCPTMS took place in a Yield Engineering System (Lawrenceville, CA) chemical vapor deposition oven (YES 1224P) that had been internally plasma cleaned and purged/seasoned with MCPTMS.²¹

Three processes were explored to determine the best deposition procedure. All were performed at 150 °C. In the first process, 1 mL of liquid MCPTMS was added to the evacuated chamber of the YES oven for 5 min. The second process was the same as the first, but the discs were left in the nitrogen-purged oven for 15-20 min after coating. The third process used the same method as the first but was followed by the introduction of 0.3 mL of liquid water for 5 min. After removal of each set of MCPTMS-coated surfaces from the oven, the discs were immediately immersed in high purity water to protect them from contamination while awaiting gold deposition.

Prior to gold deposition, discs were taken from a water storage bath and dried under a stream of dry nitrogen. Approximately 90 nm of gold (.9999 purity) was then thermally evaporated onto the discs, after which they were removed and stored for testing. Gold deposition took place in the Integrated Microfabrication Lab at BYU. Samples were tested for gold adhesion with the “Scotch tape” test; a piece of tape was attached to the gold surface and peeled away.

To more fully characterize the fabrication procedures, three batches of 5 x 5 mm² pieces of silicon (100) wafers were cleaned and coated with MCPTMS under the same conditions as the fused silica discs, but these pieces were not coated with gold. The MCPTMS coated silicon samples were characterized by contact angle goniometry (model 100-00, Ramé-Hart Instrument Co., Netcong, NJ) to probe surface wetting, time-of-flight secondary ion mass spectrometry (ToF-SIMS) (model TOF-SIMS IV, ION-TOF GmbH, Münster, Germany) for surface mass spectrometry, X-ray photoelectron spectroscopy (XPS) (Surface Science SSX-100, Surface Science Laboratories, Mountain View, CA) for surface elemental composition, atomic force microscopy (AFM) (Veeco Dimension V Scanning Probe Microscope, Plainview, NY) for

surface roughness, and spectroscopic ellipsometry (M-2000D, J.A. Woollam Co., Lincoln, NE) for film thickness.

Our vibrationally resonant sum-frequency generation (VR-SFG) spectroscopy set-up is based on a Ti:sapphire laser (Quantronix, Integra C, East Setauket, NY) with pulse widths of ~ 130 fs, 2.7 mJ per pulse and a repetition rate of 1 kHz. Most of the light enters a broad band IR optical parametric amplifier (Quantronix, TOPAS-C) to produce ca. 23 mJ of 250 cm^{-1} wide IR light centered at ca. 2900 cm^{-1} . The other portion of visible light from the Ti:sapphire laser is spectrally narrowed using a Fabry-Pérot étalon to produce a narrow band (10 cm^{-1}) visible pulse centered at ca. 792 nm. The polarizations of the visible and IR beams were *s* and *p*, respectively, resulting in *s*-polarized SFG. (All SFG spectra were collected in the *s*-SFG, *s*-visible, and *p*-IR polarization combination.) SFG signal was collected using a spectrometer (Andor Shamrock) and CCD (Andor iDus). A short-pass filter was used to remove the 792 nm light before detection.

ToF-SIMS data from three Si samples created under the same conditions described above were characterized by principle component analysis (PCA)²² using software (the PLS_Toolbox) from Eigenvector Research (Wenatchee, WA). Peak areas of ten negative ions were selected: H^- , C^- , CH^- , O^- , OH^- , C_2H^- , S^- , SH^- , SO_2^- , SO_3^- . A data matrix containing the data from each of nine samples in rows was created, and the data from each sample were normalized (a row operation) to remove the effects of different analytical conditions, such as analysis time, sample position in the instrument, fluctuations in instrument signal intensity, etc. The data were then mean centered (a column operation). After this pretreatment, PCA was performed on the matrix. Autoscaling (also a column operation), which is mean centering followed by division by the standard deviation of the data, was also performed on the normalized data in the place of mean centering alone.

3.3 Results and Discussion

3.3.1 Importance of Reference Spectra

When using a reference material for VR-SFG spectroscopy, extreme care must be taken to ensure that the reference surface is not contaminated, as this will lead to erroneous results (vide infra). To illustrate how contamination of the reference material can affect the collected data, we simulated an SFG spectrum with two peaks at 2890 and 2842 cm^{-1} , both with linewidths of 10 cm^{-1} and amplitudes of unity (Figure 3.2). We then corrected their intensities with IR profiles measured from two gold mirrors, where the actual IR spectrum was the same, coming from the same source. One of the profiles had a mostly Gaussian line shape, whereas the other had a dip at 2842 cm^{-1} , likely due to contamination. The positions of the peaks in our simulated spectrum were chosen to line up with the maximum of the IR profile and the dip at 2842 cm^{-1} . When the simulated SFG spectrum is corrected for the broadband IR intensity profile, the relative intensities of the two modes change. However, the dip in one of the profiles leads to a further increase in the peak at 2842 cm^{-1} . The corrected amplitudes are different by ca. 20%, which would likely lead to a different interpretation of the structure of this interface. Even though it is possible to produce a fit to the IR profile and remove the features due to contaminants, this will also introduce some uncertainty in the relative intensities of spectral features. Ultimately, the quality of the reference mirror affects the quality of the experimental data, hence the need for back-surface mirrors that are free of spectral contamination

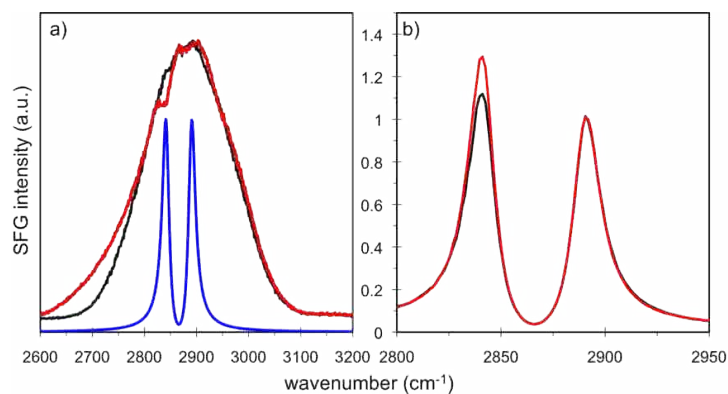


Figure 3.2. (a) IR profiles from two gold mirrors, one that is mostly smooth across the spectrum (black) and one with a spectral interference feature at 2842 cm^{-1} (red). Also shown is a fabricated SFG spectrum (blue) with a peak that overlaps the feature at 2842 cm^{-1} . (b) Fabricated SFG spectra corrected with the two IR profiles. The dip in the red spectrum leads to a corruption of the relative intensities in the corrected spectrum.

3.3.2 Unsuccessful Attempts to Make Stable Back-Surface Gold Mirrors

In our first attempt to make back-surface gold mirrors, we did not use an adhesion layer. Fused silica discs were simply cleaned with an O₂ plasma (18 W in a Harrick PDC-32G plasma cleaner, Ithaca, NY) and gold was thermally evaporated onto its surface. A protective layer of silicon nitride was added over the gold in an effort to improve its durability. This method was somewhat successful, although there were some inconsistencies in spectral features from mirror to mirror even within the same batch. (See Figure 3.3a.) Some of this inconsistency may arise from contamination of the surface prior to coating with gold. Although the gold deposition took place in a clean room facility, there was a delay of ca. 45 min between surface cleaning and gold deposition during which the samples were exposed to ambient air. One or two of these mirrors gave a smooth, roughly Gaussian profile, but most did not. The major problem with these mirrors, however, is that they all failed the “Scotch” tape test, which in spite of its simplicity is a stringent test of adhesion; transparent tape removed all the gold under it in a peel test.

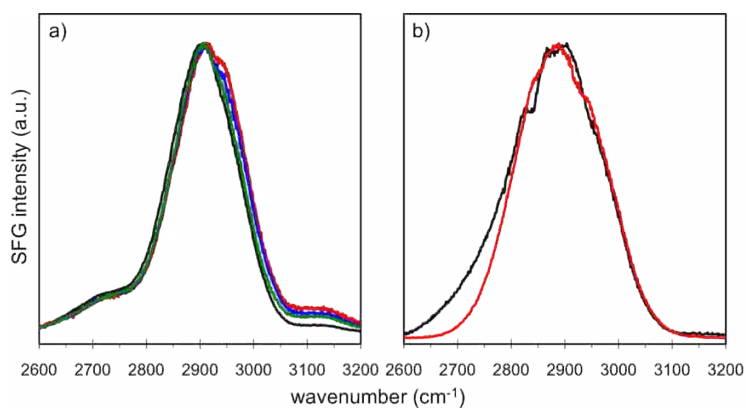


Figure 3.3. VR-SFG spectra of (a) 4 back-surface gold mirrors with no MCPTMS; (b) back-surface gold mirrors with MCPTMS that were exposed to air for ca. 45 min (black) or exposed to VUV light (red) before gold deposition.

In our next attempt, we used MCPTMS as the adhesion promoter. Discs were cleaned in *piranha* solution, coated with MCPTMS, and transported to the gold deposition chamber while exposed to the air. Figure 3.3b shows a typical SFG spectrum from this batch of mirrors. There are 3 noticeable features at 2845, 2890, and 2950 cm^{-1} , indicating that there may be either contamination of the adhesion layer/surface or incomplete crosslinking of the MCPTMS. A few mirrors gave smooth spectra, but this fabrication procedure was not reliable. Nevertheless, all discs prepared in this manner exhibited excellent adhesion; all mirrors passed the peel test.

In an attempt to remove the spectral features from the adhesion layer in the gold profile, a simple masking/etching process was attempted. Discs coated with MCPTMS were partially covered with a metal washer and exposed to 172 nm VUV (Resonance Ltd, Ontario, Canada) light for ca. 10 min prior to gold deposition. Exposure to VUV light and the concomitant ozone it produces was intended to oxidize or remove the MCPTMS layer in the center of the mirror and hence improve the spectral profile, while preserving the adhesion of the MCPTMS around the perimeter of the disc. This procedure was unsuccessful. The spectral profiles had two unwanted features at ca. 2845 cm^{-1} and ca. 2950 cm^{-1} (Figure 3.3b), probably due to VUV degradation products or other contamination. (The discs were exposed to air for ca. 15 min prior to gold deposition.) These discs also showed very poor adhesion of gold and failed the tape test with complete removal of the gold layer, even at the perimeter of the disc, presumably because of diffusion of ozone, reflection of the UV light under the masked area, or surface contamination.

These attempts revealed some important considerations in the fabrication of back-surface mirrors. First, MCPTMS works well as an adhesion promoter. Second, it appears that a common problem with all these procedures is surface contamination caused by exposure to air. In the next round of experiments, greater attention was paid to surface cleanliness.

3.3.3 Successful Attempts to Make Stable Back-Surface Gold Mirrors

Once we identified surface contamination as a possible problem in our fabrication procedures, we kept the cleaned and/or MCPTMS-coated discs immersed in ultrapure water between cleaning/coating procedures to minimize contamination from the air. Three processes were attempted, where again we took great care to keep the discs clean during all steps of the fabrication. In the first process, MCPTMS was vapor deposited by CVD, and immediately after coating, the samples were immersed in water for transport to the gold evaporation system. In the second procedure, the MCPTMS-coated discs were left in the heated CVD system for an additional 15-20 min after coating in the hope that additional curing (cross-linking) might take place. In the third procedure, 0.3 mL of water was added to the system for 5 min after CVD of MCPTMS, again to promote cross-linking of chemisorbed MCPTMS molecules and remove residual methoxy groups. After the second and third MCPTMS coating procedures, the samples were again immediately immersed in water and kept under water until just prior to coating with Au.

Table 3.1 shows surface characterization of the Si samples that underwent the three MCPTMS deposition procedures. The water contact angles and the ratio of S/Si from XPS are almost the same for all three processes, suggesting that similar amounts of MCPTMS were deposited. AFM roughness measurements showed that gas phase deposition of MCPTMS led to almost no roughening of the surfaces, i.e., all MCPTMS layers are nearly as flat as the bare (uncoated) silicon surface (0.103 ± 0.010 nm). Similar surfaces of excellent flatness have previously been observed in the CVD of 3-aminopropyltrimethoxysilane, 3-aminopropyldimethylmethoxysilane, and 3-aminopropyldiisopropylsilane on Si/SiO₂

substrates.²³ There was some variability observed in MCPTMS thickness, although all thicknesses point to deposition of monolayer quantities of MCPTMS.

Time-of-flight secondary ion mass spectrometry (ToF-SIMS) was also used to characterize these surfaces. To better understand the resulting multivariate spectra, a principal components analysis (PCA) of the negative-ion ToF-SIMS data from these surfaces was performed. In the first analysis, the data were preprocessed by normalization followed by mean centering. PC1 captured 85.17% of the variation in the data and PC2 captured an additional 14.04%. Based on the scores of the data points (spectra) on PC1 and PC2, the nine samples (three spectra from each of the three MCPTMS depositions) could not be separated. In the second analysis, autoscaling was used in the place of mean centering because it will allow the variations in the signals from the different ions to be equally important in the analysis, i.e., the analysis will not be dominated by the signals from ions with larger variances as is the case with mean centering – autoscaling is arguably a more appropriate preprocessing method for these data. As expected, for PCA of the autoscaled data, more PCs were required to capture the variation in the data: PC1, PC2, and PC3 accounted for 53.98%, 28.40%, and 16.43% of the variation in the data, respectively. Interestingly, this second analysis suggests a difference between the first three spectra, which came from the first MCPTMS deposition, compared to the other two (extra time or addition of water to the deposition chamber). Using a statistical test based on a null hypothesis, the scores on PC1 of the first three spectra were determined to be different from the remaining six spectra at a 99% confidence level. These results are interesting because they suggest that keeping the samples in the deposition chamber for a longer period of time has some effect on the samples, i.e., there may be some validity to the ellipsometry results obtained in Table 3.1.

Representative VR-SFG spectra of the gold mirrors made with the MCPTMS adhesion promoter are shown in Figure 3.4. The mirrors previously prepared without an adhesion layer are included again for comparison. Note the absence of excess features in the region of the aliphatic CH stretch modes (2800 – 3000 cm^{-1}). All three batches of mirrors made with MCPTMS exhibit similar spectra and appear to be consistent within each batch and from batch to batch. The variations between mirrors are likely due to small differences in fabrication and slight changes in alignment of the optical system.

We are unable to say whether there are residual unreacted methoxy groups in the MCPTMS layer. The absence of methyl peaks in our spectra may result from two possibilities. Either the surface density of methoxy groups is too low, or they have no orientational order. In either case, VR-SFG spectroscopy will not detect these groups. We also see no sign of methylene resonances from the C_3 backbone of the MCPTMS. This is not surprising, given that the chains are short and likely not well-ordered, again making them effectively invisible to VR-SFG.

The absence of peaks from the MCPTMS layer indicates the usefulness of these mirrors as a spectroscopic reference. All three types of mirrors also exhibit excellent gold adhesion, as determined with the tape test. Only after >20 min of exposure to O_2 plasma followed by sonication in water and CHCl_3 for >10 min each did the “Scotch” tape begin to remove the gold layer. Even after this harsh treatment, the amount of gold removed by the tape was minimal.

3.3.4 Use as a Spectroscopic Reference

Figure 3.5 shows VR-SFG spectra of octadecyltrichlorosilane (OTS), which is commonly used as a stationary phase in RPLC. The spectra have been corrected with IR profiles determined from each mirror in the four processes (1 w/o MCPTMS and the 3 with MCPTMS). The four sets of spectra have similar relative intensities. The largest differences in the peaks at $\sim 2873 \text{ cm}^{-1}$ and

$\sim 2936\text{ cm}^{-1}$ are given as a percentage in Table 3.2. The intensities from the batches with the silane adhesion layer differ by at most 5.5%; the gold mirrors with no adhesion layer show 10% variability. Not only does the MCPTMS improve the durability of the mirrors, it actually produces a better spectroscopic reference.

It also appears that the simplest procedure (Process 1) is the most effective. The variation in peak intensity in the corrected spectra is the least for this batch of mirrors. Use of additional heat or water does not lead to a more durable or spectroscopically uniform reference mirror.

3.4 Conclusions

We have produced and characterized gold mirrors fabricated with MCPTMS as an adhesion promoter. These mirrors have the advantage of not using the typical chromium adhesion film between the gold and fused silica, meaning they can be used as either front- or back-surface mirrors. We have also demonstrated the usefulness of these mirrors as a reference for VR-SFG studies of buried interfaces. There appears to be little or no interference in the nonresonant SFG profile from the adhesion layer. The MCPTMS adhesion layer also provides good long-term durability of the gold mirror.

The use of MCPTMS may lead to greater availability of back-surface gold mirrors. Mirrors made in this fashion could be used in situations where contact with fused silica would be more advantageous than contact with gold. This method could be used with any substrate that has free silanol groups at the surface, such as fused silica, silicon, quartz or BK7 glass. Gold mirrors made with a MCPTMS adhesion layer should have high reflectance for other visible and near-IR spectroscopic applications. Usefulness further into the IR than about 2500 cm^{-1} is limited by absorbance in the fused silica substrate. Protection techniques, such as coating with MgF_2 , could also be used to further enhance the durability of these mirrors.

Acknowledgments. Alexander D. Curtis helped in the preparation of some of the early mirrors without MCPTMS, and is thanked as well for helping maintain the VR-SFG system. Jim Fraser, director of the BYU Integrated Microfabrication Lab, is thanked for assistance in the gold deposition. MRL thanks Yield Engineering Systems (Livermore, CA) for their financial support. This work was supported in part by the Air Force Office of Scientific Research Young Investigator Research Program (YIP), award FA9550-09-1-0142 (JEP).

Table 3.1. Surface characterization of MCPTMS adhesion layers from three deposition processes. Thickness as measured by spectroscopic ellipsometry. Water contact angle as measured with a contact goniometer. S/Si ratio as measured by XPS. Surface roughness as measured by AFM.

Process	Thickness	Water contact angle	S/Si ratio	Roughness
1	$6.4 \pm 0.1 \text{ \AA}$	60°	0.19 ± 0.01	$0.12 \pm 0.00 \text{ nm}$
2	$10.6 \pm 0.9 \text{ \AA}$	60°	0.20 ± 0.01	$0.10 \pm 0.00 \text{ nm}$
3	$10.3 \pm 2.3 \text{ \AA}$	60°	0.19 ± 0.02	$0.13 \pm 0.03 \text{ nm}$

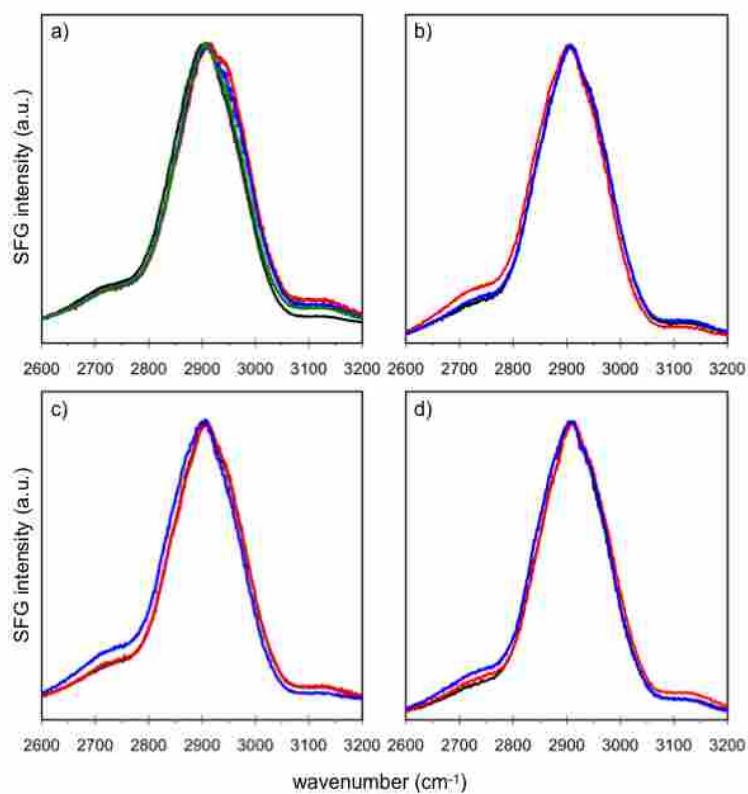


Figure 3.4. Measured IR profiles from each of the four types of gold mirrors: (a) without MCPTMS (4 mirrors), (b) MCPTMS (3 mirrors), (c) MCPTMS and heat (3 mirrors), (d) MCPTMS and water (3 mirrors).

Table 3.2. Variation in OTS peak intensity with different batches of back-surface gold mirrors.

(Spectra were corrected for the profile of the broad-band IR source.)

Wavenumber (cm ⁻¹)	No MCPTMS	Process 1	Process 2	Process 3
2873	10.46 %	2.02 %	4.70 %	5.45 %
2936	5.25 %	0.27 %	1.00 %	5.53 %

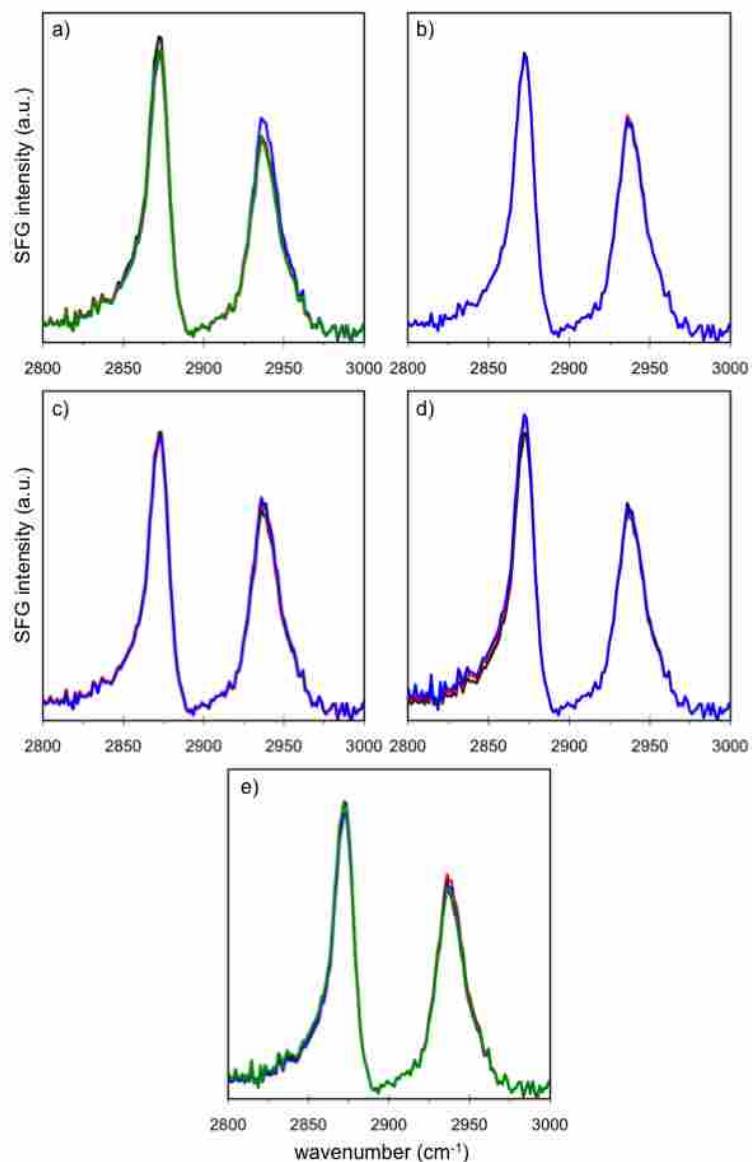


Figure 3.5. (a-d) VR-SFG spectra from a single OTS sample corrected with the IR profiles from each back-surface mirror in the four different batches (from Figure 4). (e) Averages of the corrected OTS spectra from each of the panels (a-d) plotted together. The differences in the corrected spectra are comparable to the noise level.

3.5 References

1. A.D. Quast, F. Zhang, M.R. Linford, J.E. Patterson, *Appl. Spectrosc.* 65 (2011) 634.
2. X.D. Zhu, H. Suhr, Y.R. Shen, *Phys. Rev. B* 35 (1987) 3047.
3. L.J. Richter, T.P. Petralli-Mallow, J.C. Stephenson, *Opt. Lett.* 23 (1998)1594.
4. J.B. Mcgee, (Dow Corning Corp., USA). Application: US, 1982, p 9 pp Cont
5. J.J. Ponjee, J.W.A. Nelissen, C.J.A. Verwijlen, Office, U.S.P., Ed.; U.S. Philips Corporation, New York, N.Y. 1985; Vol. 4521444, p 3.
6. Y. Tai, A. Shaporenko, H. Noda, M. Grunze, M. Zharnikov, *Adv. Mat.* 17 (2005) 1745.
7. J. Singh, J.E. Whitten, *J. Phys. Chem. C* 112 (2008) 19088.
8. C.A. Goss, D.H. Charych, M. Majda, *Anal. Chem.* 63 (1991) 85.
9. R.J. Tremont, G. Cruz, C.R. Cabrera, *J. Electroanal. Chem.* 558 (2003) 65.
10. S. Sawada, Y. Masuda, P.X. Zhu, K. Koumoto, *Langmuir* 22 (2006) 332.
11. M. Ben Ali, F. Bessueille, J.M. Chovelon, A. Abdelghani, N. Jaffrezic-Renault, M.A. Maaref, C. Martelet, *Mat. Sci. & Eng., C* 28 (2008) 628.
12. H. Park, A. Kim, C. Lee, J.S. Lee, J. Lee, *Appl. Phys. Lett.* 94 (2009) 3.
13. X. Liu, Q. Wang, L.P. Chen, *Appl. Surf. Sci.* 255 (2009) 3789.
14. S. Oleksandrov, J. Lee, S. Lee, M.G. Lee, H.Y. Choi, C.H. Chung, *J. Nanosci. Nanotechnol.* 9 (2009) 7481.
15. A. Scott, J.E. Gray-Munro, *Thin Solid Films* 517 (2009) 6809.
16. A. Riskin, C. De Dobbelaere, K. Elen, J. D'haen, H. Van Den Rul, J. Mullens, A. Hardy, M. K. Van Bael, *Phys. Status Solidi A* 207 (2010) 864.
17. A.F. Scott, J.E. Gray-Munro, J.L. Shepherd, *J. Colloid Interface Sci.* 343 (2010) 474.

18. I. Doron-Mor, Z. Barkay, N. Filip-Granit, A. Vaskevich, I. Rubinstein, *Chem. Mat.* 16 (2004) 3476.
19. A.K. Mahapatro, A. Scott, A. Manning, D.B. Janes, *Appl. Phys. Lett.* 88 (2006) 3.
20. E. Finocchio, E. Macis, R. Raiteri, G. Busca, *Langmuir* 23 (2007) 2505.
21. G. Saini, K. Sautter, F.E. Hild, J. Pauley, M.R. Linford, *J. Vac. Sci. & Technol., A* 26 (2008) 1224.
22. L. Yang, Y. Y. Lua, G. L. Jiang, B. J. Tyler, M. R. Linford, *Anal.Chem.* 77 (2005) 4654.
23. F. Zhang, K. Sautter, A.M. Larsen, D.A. Findley, R.C. Davis, H. Samha, M.R. Linford, *Langmuir* 26 (2010) 14648.

Chapter 4

Understanding Stationary Phase Structure at the RPLC Interface with VR-SFG

4.1 Introduction: VR-SFG and Nonresonant Interference

Previous work to understand the structure of the RPLC stationary phase was mostly done with narrow band nanosecond VR-SFG systems. These systems provide relatively high signal-to-noise and sub-wavenumber spectral resolution. Horn, Goates, and Bain worked ten years ago at Oxford University investigating model RPLC stationary phase structural changes under different solvent conditions at ambient pressures.^{1,2} Messmer and coworkers also worked with a similar VR-SFG system at Lehigh University in Pennsylvania. Messmer's group worked to understand sample preparation, monolayer formation, solvent ordering,³ and stationary phase structural orientation. Both groups noted changes in the stationary phase structure under a variety of mobile phase compositions at ambient pressures. These changes were attributed to various degrees of ordering of the C18 chains as well as changing chain tilt angles.⁴

While useful, work with these model RPLC systems at ambient pressures does not tell the complete story. Elevated pressures are typical in LC separations, and the stationary phase structure may have different conformations at various pressures. *In situ* work to understand the influence of stationary phase structure on retention should incorporate various mobile phase compositions as well as elevated pressures. In this chapter, I will examine the effect of nonresonant interference in VR-SFG spectra of model RPLC interfaces at ambient and elevated pressures.

One possible complication in VR-SFG spectra of the model RPLC interface not previously dealt with is the influence of nonresonant signal arising from the surface of model RPLC interfaces. The VR-SFG signal has two parts, resonant and nonresonant. These two parts arise from the origin of the SFG signal shown in equation 4.1.

$$I_{SFG} \propto |\chi_{NR}^{(2)}|^2 + |\chi_R^{(2)}|^2 + 2|\chi_{NR}^{(2)}|^2 |\chi_R^{(2)}|^2 \cos[\phi - \delta(\omega)] \quad (4.1)$$

The second order non-linear susceptibility, $\chi^{(2)}$, has resonant and nonresonant parts, which interfere with each other depending on the phase term, $[\phi - \delta(\omega)]$, where ϕ and $\delta(\omega)$ are the phase terms of the resonant and nonresonant portions, respectively, of the SFG signal.⁵ This interference of resonant and nonresonant terms corrupts the real resonant amplitudes because we do not know the phase relationship of $|\chi_{NR}^{(2)}|$ and $|\chi_R^{(2)}|$. Because we are primarily interested in the resonant SFG signal, the nonresonant influence on the resonant SFG signal must be investigated.

In equation 4.1, if the resonant or the nonresonant terms are zero, then the cross term is eliminated and we are left with either resonant or nonresonant signal alone. This brings up a very important question. Although much SFG work has been done on metallic substrates that produce a large amount of nonresonant signal, are there interfaces that exhibit negligible nonresonant signal in a region where resonant peaks are present?⁶ If the signal arising from the interface has negligible nonresonant response, then any signal generated from the surface should contain only resonant information. Our present work with fused silica is an ideal surface to test the hypothesis that fused silica has a weak nonresonant response.

We have examined several model RPLC interfaces with a broadband SFG instrument. This instrument allows us to probe the free induction decay of the resonant signal. By delaying to different points in the time domain, we can determine if changes in the overall SFG signal are due to the longer lived resonant modes or the short lived nonresonant interference with the resonant modes. When the two fundamental pulses impinge simultaneously on the surface, we call this “ $t = 0$ s”. Visible delay after the start of the IR pulse on the sample is measured in picoseconds (ps). For example, if the visible pulse is delayed 1 ps after the IR pulse impinges on the surface, we would label the spectra as “ $t = 1$ ps” or a “1 ps” delay. This approach is called time delay SFG, and it will allow us to determine if apparent structural changes are actually occurring.⁷

We used time delay SFG to examine the polymeric OTS surface and the apparent structural changes observed in different solvent environments. In an effort to examine systems more relevant to RPLC we also examined this system at elevated hydrostatic pressures typical of pressures at the column outlet. Hopefully, by examining this specific system, we can improve future research to further investigate these model RPLC interfaces.

4.2 Experimental

Materials and VR-SFG Instrumentation: Described in detail in Chapter 2

4.3 Results and Discussion

4.3.1 Delay Stage Reproducibility

To be confident that we can reproducibly move to different points in the time domain, we examined a polymeric OTS sample and a monomeric ODMS sample in air at two different delay settings 2.04 ps apart (all spectra were acquired with the *ssp* polarization combination). The delay was adjusted by moving a mechanical micrometer with markings measured in inches. The

screw was marked at 0.1", 0.01", and 0.001" increments and adjustments were only made on markings (there were no spectra taken in between marks on the delay stage). The 0 s delay stage setting was taken to be the point at which maximum nonresonant signal was obtained on a gold mirror.

Figures 4.1 and 4.2 show the results of 10 spectra for each sample; 5 at a delay of 0 ps and 5 at a delay of 2.04 ps. Spectra at the same delay time were averaged together and the standard deviation of those five spectra was plotted with the averaged spectrum. The noise in the respective spectra is the same as in the plot of the standard deviation. The low noise at the same frequency as the resonant signal is a good check for the reproducibility of the delay stage because it suggests that the positioning error of the visible delay stage does not significantly affect the observed spectra.

4.3.2 Changes in Polymeric Structure in Air at Various Visible Delays

Figure 4.3 shows a polymeric sample exposed to air at different delay times. At a delay of 0 s, there appear to be two strong peaks at 2885 cm^{-1} and 2950 cm^{-1} . Notice that the relative intensities of the two peaks change with delay. The Fermi peak at 2950 cm^{-1} changes intensity and shape with delay from a more derivative line shape to a Gaussian line shape. This would seem to indicate the presence of a significant amount of nonresonant background interfering with the resonant signal. The apparent blue shift in the spectra is also attributed to the interference of the nonresonant background.

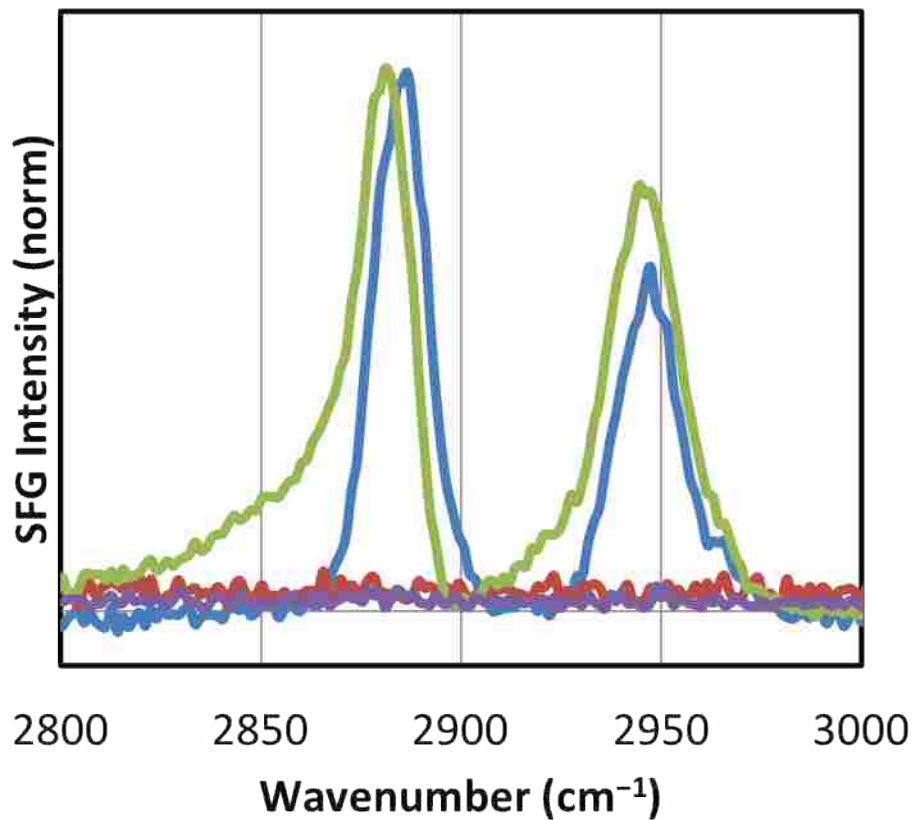


Figure 4.1. Polymeric ODS exposed to air. Repeatability of the delay stage positions is investigated at two positions. (Green) Average of 5 spectra at $t = 0$ s; (Red) standard deviation of 5 spectra at $t = 0$ s; (Blue) average of 5 spectra at $t = 2.04$ ps; (Purple) standard deviation of 5 spectra at $t = 2.04$ ps.

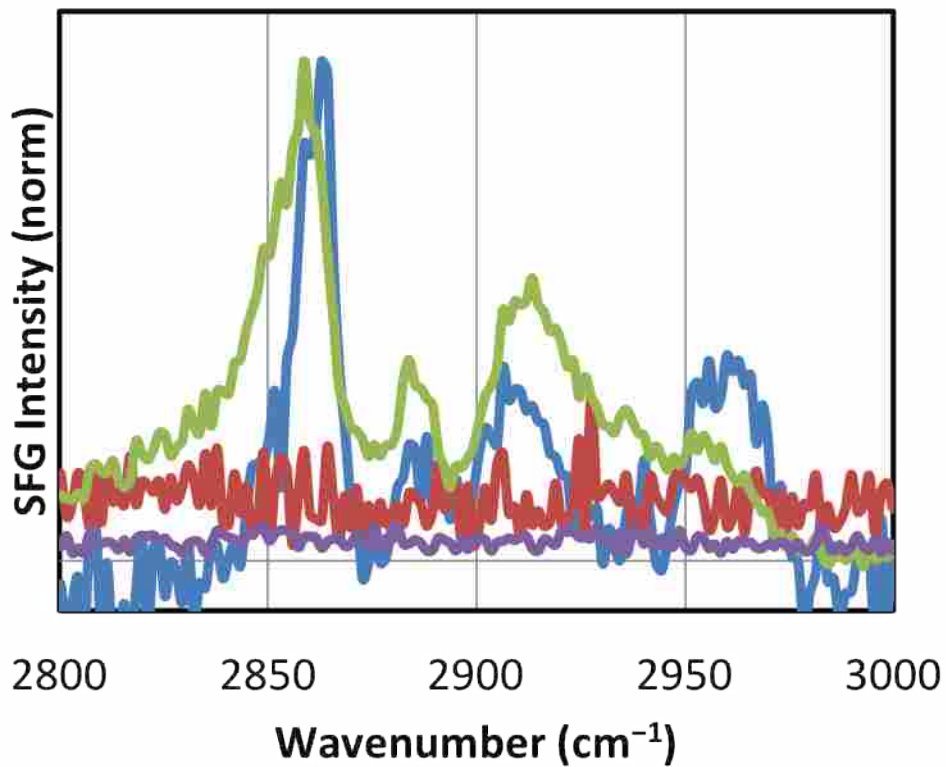


Figure 4.2. Monomeric ODMS exposed to air. Repeatability of the delay stage positions is investigated at two positions. (Green) Average of 5 spectra at $t = 0$ s; (Purple) standard deviation of 5 spectra at $t = 0$ s; (Blue) average of 5 spectra at $t = 2.04$ ps; (Red) standard deviation of 5 spectra at $t = 2.04$ ps.

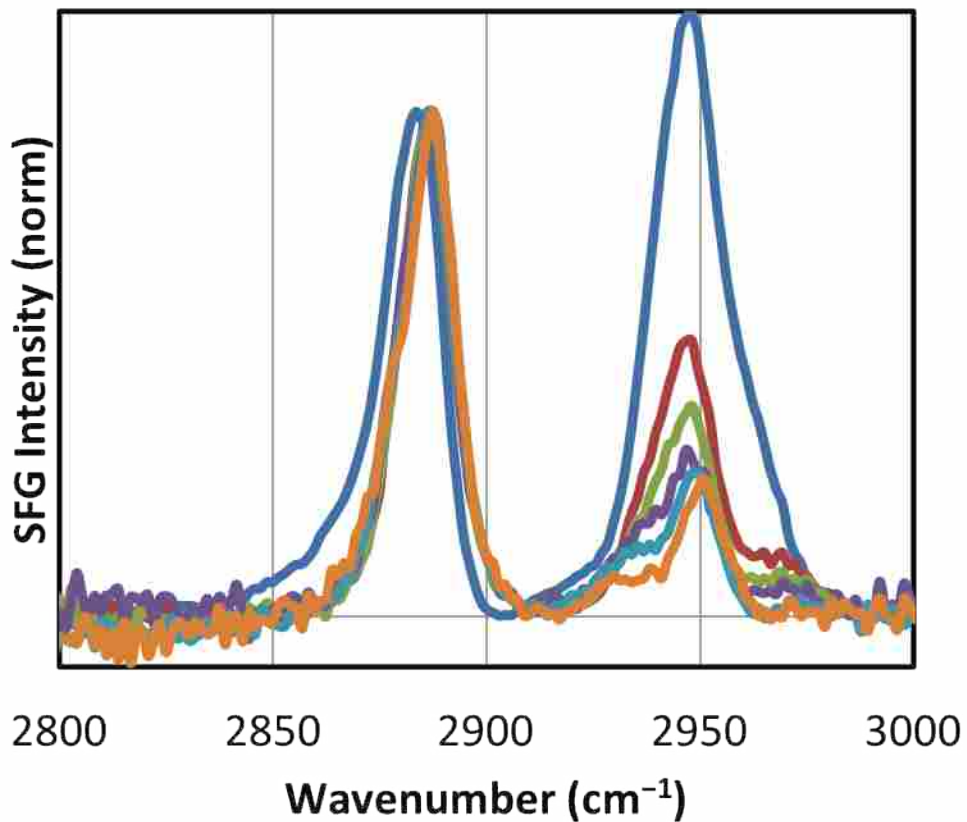


Figure 4.3. Polymeric ODS on fused silica investigated with a broadband VR-SFG system where the visible pulse has been delayed after the IR pulse. This sample was examined in air. (Blue) 0 ps; (Red) 1.86 ps; (Green) 2.04 ps; (Purple) 2.20 ps; (Turquoise) 2.4 ps; (Orange) 2.54 ps.

The delayed spectra show at least 5 peaks present at different delay times. At a delay of 2.20 ps, it is clear that the peak at $\sim 2950\text{ cm}^{-1}$ is composed of at least three modes with different phases which interfere with each other to different extents. Figure 4.3 clearly shows the non-negligible contribution of the nonresonant background with the resonant vibrational modes. This is very important because, if we interpreted the structure of the OTS monolayer at a delay of 0 s, we would have a dramatically different orientation than at a delay of 2.54 ps.

None of these delayed spectra contain all of the information necessary to determine absolute molecular orientation. At 0 s, we should be able to determine absolute orientation from relative peak intensities, but we cannot because the nonresonant background interferes with the resonant signal and distorts the correct peak intensities. Unfortunately, at any later time when we exclude the nonresonant signal completely from our VR-SFG spectra, we have apodized the resonant free induction decay to the extent that absolute peak intensities are unknowable. The only possible way to account for resonant and nonresonant interactions would be to obtain spectra at multiple time delays and then use Fourier transform analysis and curve fitting to extract the resonant signal from the time domain spectra.⁸

In summary, nonresonant suppression changes the observed vibrational mode intensities. To be sure that we are only probing the resonant modes, we must suppress the nonresonant signal. This suppression eliminates the interference from the nonresonant response but it also reduces our confidence in molecular orientation. Without more exhaustive analysis, we can only say that changes in the stationary phase may be occurring. We cannot determine absolute orientation of surface molecules because of the nonresonant interference.

4.3.3 Changes in Polymeric Structure under Solvent at Ambient Pressure

Figure 4.4 compares VR-SFG spectra of a sample that was stored in CD₃OD and then examined in D₂O at ambient pressures. These spectra also consist mainly of two peaks, one assigned to the symmetric methyl stretch mode at $\sim 2884\text{ cm}^{-1}$ and a Fermi resonance at $\sim 2944\text{ cm}^{-1}$. The lack of significant methylene symmetric stretch signal at $\sim 2866\text{ cm}^{-1}$ suggests that the alkyl chains are mostly all-trans and well ordered. Note also the different relative intensities of the 2884 cm^{-1} and 2944 cm^{-1} peaks. It would seem that there is a changing orientation of the polymeric OTS chains after 1.5 h immersion in D₂O.

To determine if these changes are the result of changing orientation or optical interference, we delayed the visible pulse relative to the IR pulse.^{4,5} If the delayed spectra also change with time and exposure to the D₂O, this would suggest that the structure is changing. Figure 4.5 displays spectra collected after the visible pulse was delayed 2.04 ps after the IR pulse. (Spectra in both Figures 4.4 and 4.5 at 0 h were collected within 5 min of each other, and 1.5 h were also sequential measurements at the two delay settings.)

The differences in the spectra of Figure 4.5 are within the noise level, and the apparent changes observed in Figure 4.4 seem to have disappeared. Because we are only probing resonant modes at this delay, we can be confident that the changes in Figure 4.4 were from the nonresonant signal. The source of these changes may be solvent exchange, which may change the interface, but I cannot be certain without further experiments. I can certainly say that the apparent changes in VR-SFG at a 0 s delay are not necessarily resonant changes.

Although, previous work with polymeric C18 silanes yielded similar results as displayed here, the interpretations of the spectra are somewhat suspect.⁴ Previous researchers did not

employ time delay VR-SFG. It is very possible that any observed changes may have had more to do with the nonresonant signal than with actual structural changes in the stationary phase.

4.3.4 Polymeric Stationary Phases at 900 psi in H₂O

To test whether hydrostatic pressure has an effect on the polymeric stationary phase we exposed a CD₃OD stored sample to H₂O at 900 psi. Figure 4.6 displays spectra from this sample initially and after 3 h of exposure to the higher pressure. Changes in the spectra are slight and within the noise level of the spectra, so any interpretations of a changing stationary phase under 900 psi pressure in water would be difficult to make. There are certainly no dramatic changes in the observed spectra when exposed to elevated pressures. Figures 4.7 and 4.8 display the spectrum of a similarly treated OTS sample. The lack of large changes in the delayed spectra outside of noise indicates that the changes observed at ambient pressures are not occurring on the same time scale for pressurized samples.

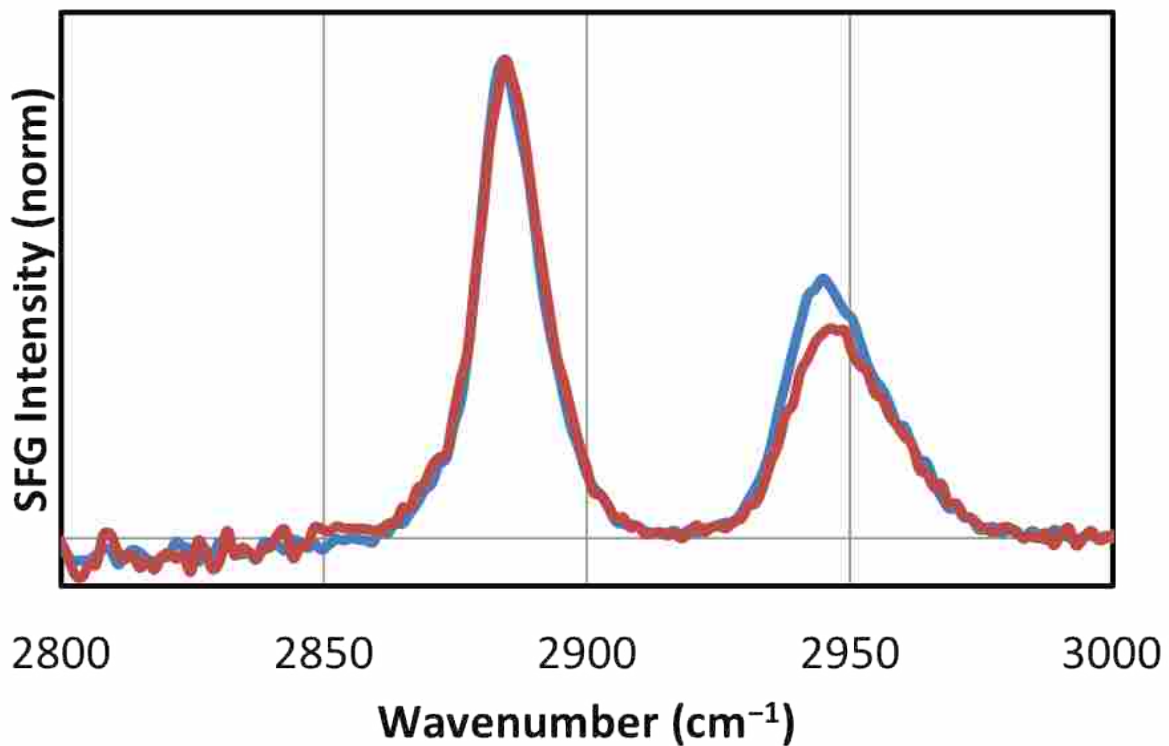


Figure 4.4. Polymeric ODS on fused silica investigated with a broadband VR-SFG system where the visible pulse is optimally overlapped in time with the IR pulse. This sample was previously stored in CD₃OD and then placed in a chamber with D₂O to investigate possible structural changes with solvent environment. (Blue) 0 h; (Red) 1.5 h.

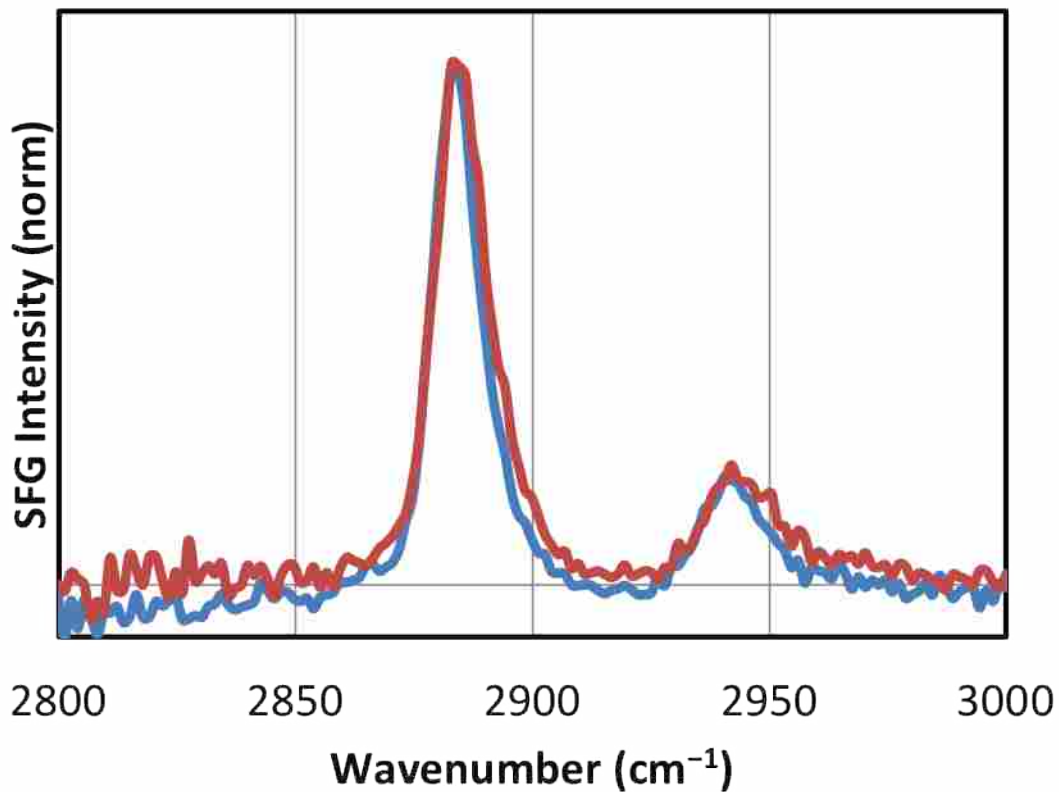


Figure 4.5. Polymeric ODS on fused silica investigated with a broadband VR-SFG system where the visible pulse has been delayed ~ 2.04 ps after the IR pulse. This sample was previously stored in CD_3OD and then placed in a chamber with D_2O to investigate possible structural changes with solvent environment. (Blue) 0 h; (Red) 1.5 h.

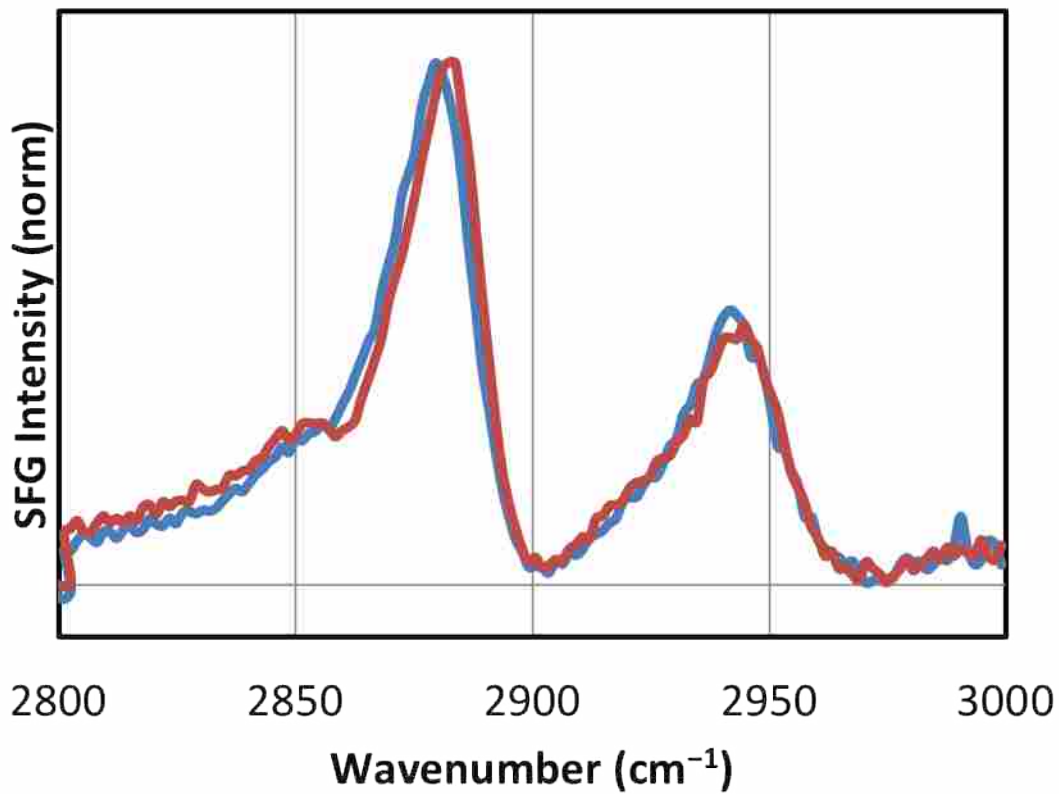


Figure 4.6. Polymeric ODS stored in CD₃OD and then placed under D₂O and immediately pressurized to 900 psi. (Blue) Initial ambient; (Red) after 3 h of hydrostatic pressure.

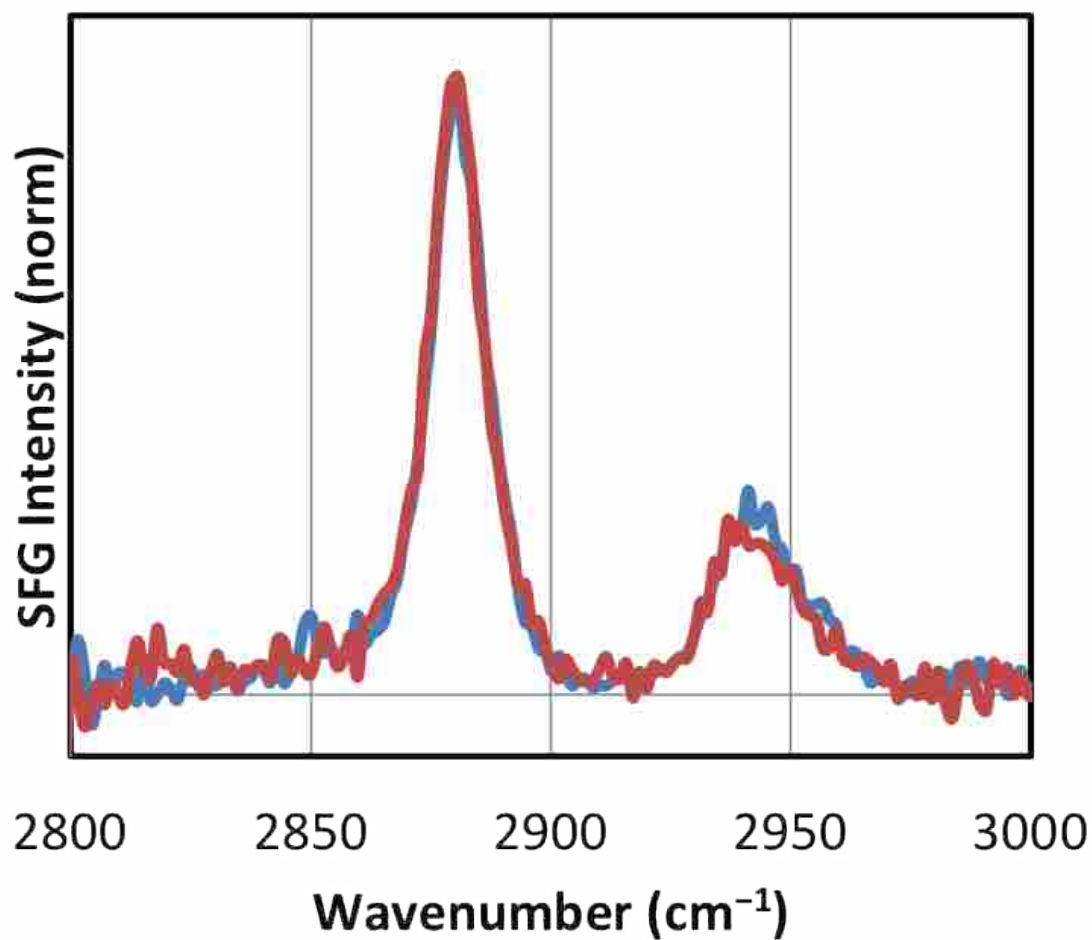


Figure 4.7. Polymeric OTS on fused silica investigated with a broadband VR-SFG system where the visible pulse is optimally overlapped in time with the IR pulse. Polymeric OTS stored in CD₃OD and then placed under D₂O and immediately pressurized to 900 psi. (Blue) Initial ambient; (Red) after 3 h of hydrostatic pressure.

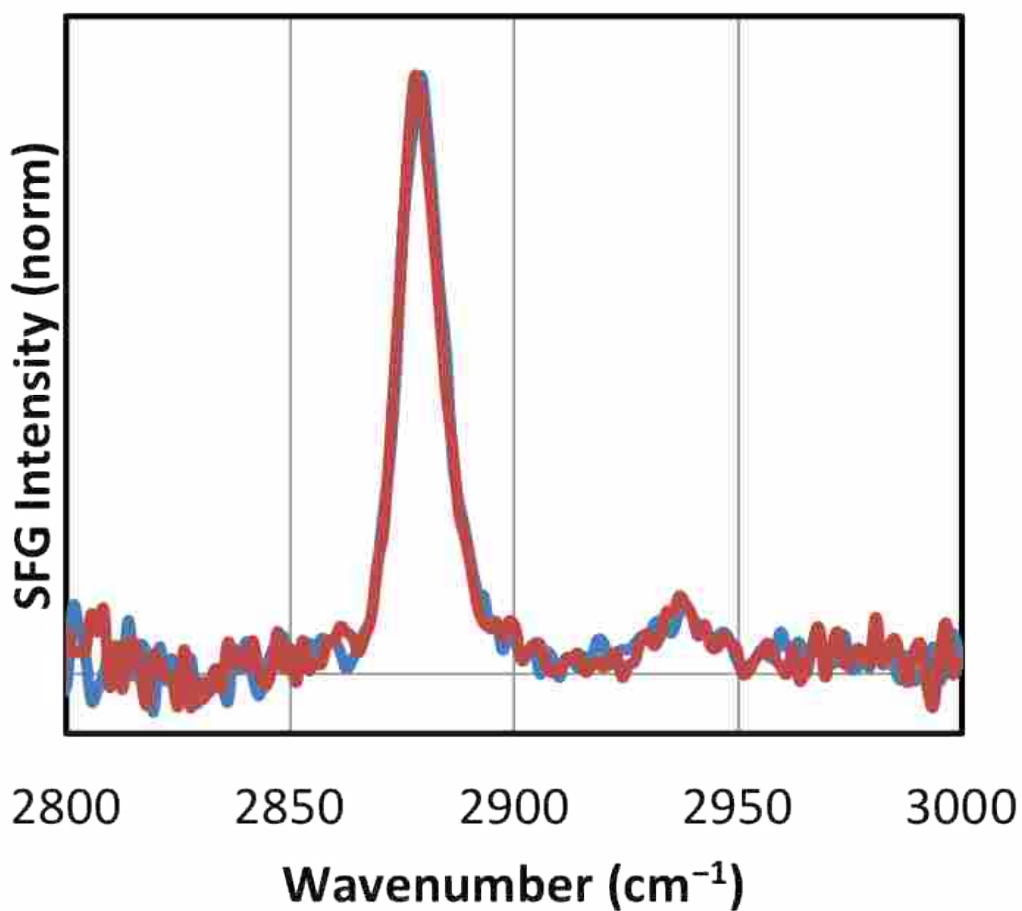


Figure 4.8. Polymeric OTS on fused silica investigated with a broadband VR-SFG system where the visible pulse has been delayed ~ 2.03 ps after the IR pulse. Polymeric OTS stored in CD_3OD and then placed under D_2O and immediately pressurized to 900 psi. (Blue) Initial ambient; (Red) after 3 h of hydrostatic pressure.

There are, however, several features of interest in Figure 4.6. From high energy to low, we see an OH peak at $\sim 3000\text{ cm}^{-1}$ that might be interfering with the resonant and nonresonant peaks at lower energies. To avoid this, we suggest that future work use D_2O to shift this OD mode to much lower frequencies. Also, the presence of defined shoulders at $\sim 2920\text{ cm}^{-1}$ and 2850 cm^{-1} would seem to suggest the presence of disordered C18 chains in this sample having gauche defects. These features are also corrupted by the clear derivative lineshapes from the nonresonant interference. The long shoulder on the low energy side of the two prominent peaks in Figure 4.6 and the sharper drops on the high energy side would suggest that this sample has a significant amount of nonresonant signal, which likely corrupted the resonant signal.

Other OTS samples seemed to have different amounts of nonresonant interference and gauche defects as well as observed changes even at elevated pressures. Under closer inspection of the pressure work that has been done with polymeric OTS, we also noted that the time between making the samples and using the samples varied drastically. We assumed that changes would occur independent of how old the samples were. This might not be true, and future work should focus on comparing samples with the same preparation history.

4.3.5 Polymeric Stationary Phases at Pressures Above 900 psi

Further work with more elevated pressures should be done because pressure studies are the most relevant for understanding any structural changes that may occur in typical RPLC separations. Some preliminary work to reach higher pressures more typical of the inlet pressures in an RPLC column has had mixed success. Samples made on 1" round 1/8" thick fused silica often broke at pressures of $\sim 1000\text{ psi}$ in a sample cell designed by Robert Baker. Figure 4.9 shows a different design using right angle prisms (Thorlabs part# PS611) in a larger sample cell that I helped to design. Using this pressure, cell I was able to reach hydrostatic pressures of

6500+ psi. One difficulty I encountered was getting light in and out. Subsequent improvements on this design might easily overcome this problem and investigating samples at very high pressures will then be possible.

4.4 Conclusions

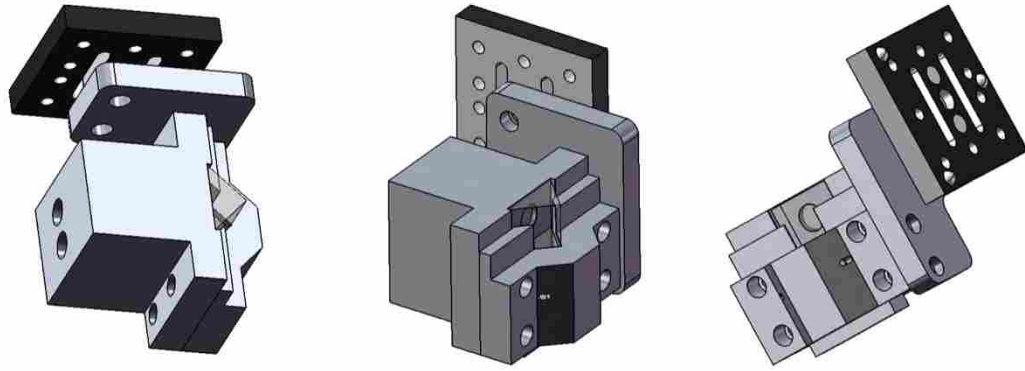
In summary, the nonresonant interference in fused silica samples is not negligible and it complicates the determination of absolute orientation in two ways. One, the intensity of the SFG signal is proportional to the modulus-squared susceptibility. Squaring the susceptibility destroys the complex values in $\chi^{(2)}$, which has both the imaginary and real parts of the resonant signal. Because both parts are necessary for proper analysis, orientation information is lost through the interference of resonant and nonresonant terms. Two, the cross term involving both nonresonant and resonant parts amplifies any nonresonant signal present at the interface. As a result, at $t = 0$ s we observe the interaction (constructive or destructive, depending on the relative phase relationship) of the resonant and nonresonant terms. Furthermore, it is impossible to separate the resonant and nonresonant responses when the visible and IR pulses are optimally overlapped.

Only if we delay the visible pulse can we exploit the different free induction decays of the nonresonant and resonant signals and separate the resonant portion of the signal. This apodization destroys absolute orientation information because the entire free induction decay cannot be observed. The nonresonant signal is (1) unknown to us both in phase and amplitude and (2) different with a variety of surface conditions.

These factors make absolute determination of surface structure very difficult using conventional VR-SFG techniques or data post processing. There are too many variables to account for, with the interactions of resonant and nonresonant signals, to really be sure about structural information from VR-SFG spectra. Data post-processing alone cannot extract the

necessary information to determine absolute molecular orientation. Even more important, we have shown that apparent changes in VR-SFG spectra are not necessarily resonant-only changes. Furthermore, changes in VR-SFG spectra should only be attributed to resonant features if we are sure that the nonresonant signal is not interfering with the resonant signal.

Fortunately, this work has provided researchers with some very useful insights into the structure of the RPLC stationary phase exposed to typical LC conditions. We have found that the OTS stationary phase does not undergo dramatic structural changes when exposed to elevated pressures. We do need to be cautious when determining whether spectral changes are actually structural changes or just nonresonant interference with both the OTS and ODMS fused silica interfaces. Finally, the structure of the RPLC stationary phase may in fact change with different mobile phase compositions but the changes we have observed are more probably due to differences in mobile phase penetration into the stationary phase. The differences in solvent polarity and other properties may be the reason for differences in chromatographic retention times. Because of this work we have discovered that there are changes occurring at the RPLC interface with the stationary phase and mobile phase. This discovery adds importance to further work that may reveal the source of these changes. The relationship that these observed changes have with RPLC retention times may have profound significance to those seeking to understand the molecular basis for retention in model RPLC systems.




	Ph. 422-4570 Fax. 422-0475 108 CTB BYU		UNLESS OTHERWISE SPECIFIED: DIMENSIONS ARE IN INCHES TOLERANCES ARE AS FOLLOWS:		DEPT. Chemistry
	www.byu.edu/ctmrl		.X .XX .XXX ANLR	.1 .01 .005 .5deg	PROJECT: 8374 Prism Mount
DRAWN T. Garrett	NAME T. Garrett	DATE 5/28/2010	MATERIAL	QTY 1	PART: Assembly Style 2
CHECKED XXXX	DO NOT SCALE DRAWING			DRAWING: Assembly Style 2	Finish Date:
					SHEET 1 OF 2

Figure 4.9. Newly designed pressure cell that holds Thorlabs right angle prism (part # PS611).

This design was able to exceed hydrostatic pressures of 6500 psi.

4.5 References

1. B.A. Horn, Dissertation: Spectroscopic Investigations Of Chromatographic Processes, Brigham Young University, Provo, UT, 2001.
2. L.R. Baker, Thesis: Spectroscopic Study Of Compressible Mobile Phase And Stationary Phase Behavior In Chromatography, Brigham Young University, Provo, UT, 2007.
3. M.C. Henry, E.A. Piagessi, J.C. Zesotarski, M.C. Messmer, *Langmuir* 21 (2005) 6521.
4. M.C. Henry, L.K. Wolf, M.C. Messmer, *J. Phys. Chem. B* 107 (2003) 2765.
5. C.D. Bain, *J. Chem. Soc., Faraday Trans.* 91 (1995) 1281.
6. T.T. Nguyen, K. Rembert, J.C. Conboy, *J. Am. Chem. Soc.* 131 (2009) 1401.
7. A.D. Curtis, S.R. Burt, A.R. Calchera, J.E. Patterson, *J. Phys. Chem. C* [Online early access]. DOI: 10.1021/jp200915z. Published Online: May 19, 2011.
<http://pubs.acs.org/journal/jpccck> (accessed Jun 13, 2011).
8. A.D. Curtis, S.B. Reynolds, A.R. Calchera, J.E. Patterson, *J. Phys. Chem. Lett.* 1 (2010) 2435.

Chapter 5

Conclusions and Afterthoughts

5.1 Structure of the RPLC Stationary Phase

When I started this work, I really just dove in, expecting to have great success. I soon learned that my results were confusing and inconsistent. I spent much of my first year on this project rethinking how I was doing things. The synthesis was my biggest challenge. After I refined the synthesis, I needed to get consistent results.

Obtaining consistent results led me to re-examine how we made our gold reference mirrors. I was sure that making reliable reference mirrors would take a month at most. Ironically, after 6 months, I was able to make reliable gold mirrors and we published a paper describing the process. Then, I was sure that everything would work according to my plans.

I got back to work and found that the literature wasn't certain about peak assignments of the C18 groups. After collaborating with a number of students in the Castle group for about a year, they were able to make deuterated molecules that would allow me to assign the different modes of the C18 stationary phases. Thanks to the Castle group's hard work, in a matter of weeks we were able to assign the various modes that are commonly observed in VR-SFG spectra of OTS bonded to fused silica.

Unfortunately, it seemed that I was only part of the way there. New work in our lab showed that there was a significant amount of nonresonant interference in the spectra I collected. This had to be better understood before I could move forward. After spending several months redoing experiments, I felt better prepared to begin working toward describing the orientation of the stationary phase of the RPLC system. And then, when I felt that I was just starting to understand things, it was time to graduate and move on.

I am not saying that the journey to understanding this model RPLC system was not enjoyable. It certainly produced wonderful results for papers and improved understanding of VR-SFG. I just did not expect these detours as I pushed to make sense of everything. Although, I feel that I have left a great deal of work for those that continue this work, I have been able to learn a few important things about this model RPLC system.

I have learned that well ordered polymeric C18 stationary phases may be too densely packed for dramatic conformational changes when exposed to different solvents. I typically observed two strong peaks in these model C18 systems. These two peaks changed in intensity with and without suppression when moved from air exposure to methanol or acetonitrile. However, under either solvent or a ratio of either solvent there do not seem to be dramatic changes in the spectra at ambient pressures or 900 psi.

The close packing of these C18 systems may confine the C18 chains so much that they are not able to change orientation. I suspect that mixed C1/C18 phases may be able to change orientation. Monomeric ODMS would also be a good system to work with because it has looser packing due to the basal methyl groups.

5.2 Gold Mirrors

In retrospect, I could have designed a much cheaper and simpler method for making back surface mirrors. The 3-MCPTMS would have attached to a clean substrate having silanol functional groups if it was deposited in a regular vacuum oven. To do this, one would simply put a dish of 3-MCPTMS in the vacuum with clean substrates. These could then be removed and coated with thermally evaporated gold. An even better option might be to thermally evaporate silver onto these substrates. Silver mirrors have better reflectivity in the 2900 cm^{-1} region and they would be cheap to produce. They might tarnish on the front surface, but that surface could

be protected to prevent oxidation, and the back surface would already be protected from oxidation by the substrate.

5.3 RPLC

Cleanliness was my biggest enemy when making C18 stationary phases. After several back and forth emails with Lauren Wolf, a Ph.D. student under Messmer, I learned that the way to get clean samples was to rinse with copious amounts of solvents and sonicate in solvents. Additionally, never allowing my samples to dry seemed to help keep them clean.

I confirmed that cleanliness was important by taking two sets of samples through the polymeric C18 coating process. One set was coated and cleaned as I have described earlier and never allowed to dry, rinsed with several solvents and cleaned with sonication. The other set was treated exactly the same way, but I did not add the C18 reagent to the methylene chloride reaction mixture. After analysis with goniometry and VR-SFG, I was able to confirm that this rigorous process was clean. Drying the samples in an oven, or letting them dry out at all, resulted in contamination and inconsistent results when examined with VR-SFG.

5.4 Pressure Work

The best approach to getting light in and out of the high pressure prism mount may be to use a counterpropagating geometry like that describing Bain's VR-SFG set-up at Oxford, and in Horn's dissertation.^{1,2} Doing so would allow for small entrance and exit slits, key for high pressures and a more obvious geometry for locating the SFG beam.

I wish the best of luck to whomever continues this work. It was exciting and engaging for me, and I have learned a great deal through solving the problems that have arisen over the years.

5.5 References

1. B.A. Horn, Dissertation: Spectroscopic Investigations Of Chromatographic Processes, Brigham Young University, Provo, UT, 2001.
2. L.R. Baker, Thesis: Spectroscopic Study Of Compressible Mobile Phase And Stationary Phase Behavior In Chromatography, Brigham Young University, Provo, UT, 2007.